2

EFFECTS OF ATMOSPHERIC AEROSOLS ON SCATTERING REFLECTED VISIBLE LIGHT FROM EARTH RESOURCE FEATURES

NASA Atmospheric Aerosols #141330-3294R-72

Final Report

Presented to

NASA supported UNIVERSITY SUSTAINING PROGRAM NGL-43-001-021

31 December 1972

by

Dr. Kenneth E. Noll and Dr. Bruce A. Tschantz
Civil Engineering Department

and

Mr. Wayne T. Davis
graduate student

ABSTRACT

The purpose of this investigation was to identify the vertical variations in atmospheric light attenuation under ambient conditions and to provide a method through which aerial photographs of earth features might be corrected to yield quantitative information about the actual features.

A theoretical equation has been developed based on the Bouguer-Lambert extinction law and basic photographic theory. This provided a relationship between the actual density of the photographic negative of an object (D_o), the density (D) of the same object at a given altitude (X), and the coefficient of extinction of light (b). This equation states that

$$\ln \left[e^{\frac{D}{.434\gamma_D}} - e^{\frac{D_B}{.434\gamma_B}} \right] - \frac{D_o}{.434\gamma_o} = -bX,$$

where γ_D, γ_B, and γ_o are determined from the measurable Hurter and Driffield characteristic curve of the photographic material. Measurements were made of the initial density produced by the energy reflected from control targets on the ground and the density produced by the energy received at flight altitudes through the use of photography. Measurements of the loss of energy at different altitudes due to light scattering in the vertical were made by an integrating nephelometer. These independent measurements were compared through the theoretical equation developed. The theoretical equation has been found to hold for the altitudes studied (altitudes up to 9000 feet above the ground) within the experimental accuracy of the experiments performed.

The overall research effort has provided the following important information.

1. It has provided a method to determine the accumulative bX between the ground and an altitude, X, based on ground density data and aerial density data. As a result the average b can be determined.
2. For remote sensing of the environment, it has provided a method through which aerial photographs of earth features can be corrected for the attenuation of light due to an aerosol layer between the ground and the altitude specified, provided the coefficient of extinction of the layer is known.

TABLE OF CONTENTS

CHAPTER PAGE

LIST OF TABLES

LIST OF FIGURES

FIGURE PAGE

CHAPTER I

INTRODUCTION

NASA has recognized the tremendous potential of remote sensing as a technique to survey the earth's resources. Their interest is demonstrated by the unmanned Earth Technological Satellite Programs (ERTS-A and ERTS-B) of 1972 and 1973, and the manned SKYLAB-A orbiting EREP workshop program scheduled for 1973. Although much "spectral signature" work has been done to identify optimum spectral bands for delineating special surfacial features, much more work is still needed to describe the effect(s) of atmospheric aerosols on scattering and attenuating the light reflected from these features. Work has been done in the past in describing the effects of aerosols on the reflected light from objects in the horizontal direction under ambient and controlled conditions. The general objective of this report was to identify the vertical variations in atmospheric light attenuation under ambient conditions and to provide a method through which aerial photographs of earth features might be corrected to yield quantitative information about the actual features.

A theoretical equation has been developed based on the Bouguer-Lambert extinction law and basic photographic theory. This provided a relationship between the actual density of the photographic negative of an object (D_o), the density (D) of the same object at a given altitude (X), and the coefficient of extinction of light (b). This equation states that

$$\ln \left[e^{\frac{D}{.434\gamma_D}} - e^{\frac{D_B}{.434\gamma_B}} \right] - \frac{D_o}{.434\gamma_o} = -bX,$$

where γ_D, γ_B, and γ_o are determined from the measurable Hurter and Driffield characteristic curve of the photographic material. Measurements were made of the initial density produced by the energy reflected from control targets on the ground and the density produced by the energy received at flight altitudes through the use of photography. Measurements of the loss of energy at different altitudes due to light scattering in the vertical were made by an integrating nephelometer. These independent measurements were compared through the theoretical equation developed. The theoretical equation has been found to hold for the altitudes studied (altitudes up to 9000 feet above the ground) within the experimental accuracy of the experiments performed.

The work described herein was performed over an eighteen-month period beginning July 1, 1971, and ending December 31, 1972. The first fifteen months were used to obtain data and analyze preliminary data. Final data analysis and the study report were completed during the last four months. Geographical areas of study were (A) artificial targets on The University of Tennessee at Knoxville campus, (B) appropriate natural targets in close proximity of Knoxville, and (C) an oil tank farm in Knoxville, Tennessee.

The overall research effort has provided the following important information:

1. It has provided a method to determine the accumulative bX between the ground and an altitude, X, based on ground density data and aerial density data. As a result the average b can be determined.
2. For remote sensing of the environment, it has provided a method through which aerial photographs of earth features can be corrected for the attenuation of light

due to an aerosol layer between the ground and the altitude specified, provided the coefficient of extinction of the layer is known.

CHAPTER II

LITERATURE REVIEW

I. THEORY OF CONTRAST

Introduction

The quality of photography and photometry, namely, the ability to distinquish between one object and a second object of different intensities; is greatly affected by the turbidity of the atmosphere. One of the more significant effects is the reduction in contrast between an object and its background. The contrast ratio is defined as the radiance or luminance of an object compared to the radiance of its background. Since any function of the contrast ratio also represents a form of contrast, there are an unlimited number of ways to represent the contrast between two objects.[1] Most of the studies involving the theory of contrast have been directed toward the attenuation of light in the horizontal direction, although some work has been done in the vertical.[2,3]

Koskmeider's Law

The basic concepts of contrast were developed by Koshmeider and his associates.[4] These concepts were based on the development and testing of the equation which became known as Koshmeider's law,[4]

$$B_x = B_o e^{-bX} + B_H(1 - e^{-bX}) \qquad \text{(II-1)}$$

where B_o is the inherent brightness of an object (brightness at zero range), B_x is the apparent brightness at range X, B_H is the apparent brightness of the background, e is the exponential base, and b is

the attenuation coefficient. Defining the basic relations of inherent and apparent contrast, respectively,

$$C_o = (B_o - B_H)/B_H$$

and

$$C_x = (B_x - B_{H_x})/B_{H_x} .$$

If the assumption is made that the background brightness is not a function of the distance ($B_H = B_{H_x}$), then from Koshmeider's law it is seen that

$$C_x = C_o e^{-bX} .$$

This is the form of the contrast theory that is most often used in experiments involving horizontal attenuation of light, since the background is generally chosen to be the horizon.

Contrast by Photographic and Photoelectric Photometry

A comparison was made of the atmospheric attenuation of the contrast as defined above by photographic and photoelectric photometry in the visible light range.[4,5]

> The procedure used . . . consisted of making brightness contrast measurements by means of telephotometers for each filter. . . . In each case the horizon brightness along a particular direction was chosen as the background brightness for the objects being photometered. In the case of the photographic photometry, the usual H and D curves were prepared for the gray scale . . . and brightnesses of the test objects and their sky backgrounds were determined from densitometric measurements using a photoelectric densitometer.

By means of the brightness data obtained using the two types of photometers, the apparent contrast of each of the objects was calculated. A graph of the $\log_e$ of the percent apparent contrast versus the range for each filter was plotted. It was found that the photoelectric and photographic measurements of the attenuation of brightness contrast were substantially the same.

Smoke Plumes Studied by Contrast Theory

Conner,[6] in a study of the transmission of light through smoke plumes, defined the inherent and apparent contrast between two targets, respectively;

$$C_{i_c} = (B_1 - B_2)/B_1 \qquad \text{(II-2)}$$

and

$$C_{a_c} = (B'_1 - B'_2)/B'_1. \qquad \text{(II-3)}$$

The quantity B_1 is the inherent brightness of the first target, B_2 is the inherent brightness of the second target, and the prime (') signifies the apparent brightness of each target. The apparent brightness can be written as

$$B'_1 = B_a + B_1T \qquad \text{(II-4)}$$

and

$$B'_2 = B_a + B_2T, \qquad \text{(II-5)}$$

where B_a is the sky-light not originating at the target, and T is the transmission of the layer. The transmission, T, of a layer can be expressed as the ratio of the brightness at distance X to the brightness at zero distance:

$$T = e^{-bX}. \qquad \text{(II-6)}$$

Thus, substituting T into the equation resulting from the subtraction of Equation II-5 from Equation II-4,

$$-bX = \ln \left[\frac{B'_1 - B'_2}{B_1 - B_2}\right]. \qquad \text{(II-7)}$$

From Equation II-7, it is shown that the attenuation coefficient can be theoretically measured in terms of the brightnesses of two targets at zero range and range X. Conner[6] has illustrated the feasibility of using both photoelectric and photographic techniques in evaluating the transmittance of smoke plumes by measuring the

luminance difference between a pair of contrasting targets through a plume ($B_1' - B_2'$) and clear of the plume ($B_1 - B_2$). Conner has suggested that there are many possible combinations of contrasting targets that may be used. Those mentioned were: (1) blue sky--white cloud, (2) high ground--sky, (3) land--horizon, (4) plowed field--wooded area, and (5) water--sandy beach. The advantage of photography as found by Conner was that it provided a permanent and instantaneous record of an event, while photoelectric photometry had the advantage of greater simplicity and faster data handling.

Conner[6] has also shown that for the situation where a target is much brighter than the surrounding background ($B_1 \gg B_2$ and $B_1' \gg B_2'$) that one need only use a single target to determine the plume transmittance. The transmittance then equals

$$T = \frac{B_1'}{B_1}.$$

Vertical Attenuation Studied by Contrast

Mazurowski[3] has studied the attenuation of brightness contrast (photographic contrast) using another variation of the concept of contrast. The inherent contrast was defined as

$$C_{i_m} = (B_o - B_H)/(B_o + B_H).$$

Since

$$B_x = B_a + B_o T,$$

then the apparent contrast at an altitude was found to be

$$C_{a_m} = C_{i_m} [1 + (B_a/T) (\bar{B}_o)^{-1}]^{-1}, \qquad \text{(II-8)}$$

where

$$\bar{B}_o = (B_o + B_H)/2.$$

Rearranging Equation II-8,

$$(B_a/T) = \bar{B}_o[(Ci_m/Ca_m) - 1]. \qquad \text{(II-9)}$$

From measurements of the luminance of a set of black, white, and gray ground targets of area 48 square feet each, Mazurowski was able to calculate values of B_a/T which were then compared and related to meteorological parameters such as[3]

> . . . ground visibility, haze-layer heights, the number and extent of temperature inversions in the atmosphere, total precipitable moisture content, vertical extent of humid layers, the polarization ratio of skylight and air mass. The visibility, total precipitable moisture content, and the polarization data yielded little relation with the observed contrast reduction.

However, it was found from this study that there was a correlation between air mass (and season of occurrence) with the contrast.

It has been shown by Veress[7] that polluted air can be effectively mapped through the application of the theory of contrast and color aerial photography using a polaraid filter. Both quantitative and qualitative information was obtained about the nature and physical dimensions of the smoke plumes studied. Topographical type maps were constructed of the polluted air masses from vertical and oblique photographs taken.

II. ATTENUATION COEFFICIENT

Bouguer-Lambert Law

The above experiments have made use of the concept of contrast to determine the transmittance of a layer of air. The measurement of the transmission of an air layer has also been studied by a more direct approach through the Bouguer-Lambert law:

$$T = \frac{B}{B_o} = e^{-bX}. \qquad \text{(II-6)}$$

The quantity B_o is the intensity or brightness of an object at zero range, and B is the intensity of the object that has been reduced by attenuation through range X. This approach involves the actual measurement of the attenuation coefficient using specific instruments.

Attenuation Coefficient

The attenuation coefficient is composed of four terms:[8]

$$b = b_{Rayleigh} + b_{abs\text{-}gas} + b_{abs\text{-}aerosol} + b_{scat}, \qquad \text{(II-10)}$$

where $b_{Rayleigh}$ is the scattering of light by air molecules, $b_{abs\text{-}gas}$ is the absorption coefficient of the gaseous components in the air (such as NO_2, O_3, H_2O), $b_{abs\text{-}aerosol}$ is the absorption coefficient of aerosols or particulate matter such as soot, and b_{scat} is the scattering coefficient due to aerosols. Charlson[8] has found that for the wavelengths of .46 to .49 micrometers (μ) that $b_{Rayleigh}$ is approximately 0.3×10^{-4} meters^{-1}. Ozone and water (H_2O) have also been found to be very weak absorbers in the visible light region.[8,9] Eltermann[10] has measured the values of $b_{Rayleigh}$, b_{scat}, and b_{ozone} for various wavelengths for a typical atmosphere. Ozone absorption was found to be of the same order of magnitude as b_{scat} at .27μ. However, at .32μ the ratio of b_{scat} to b_{ozone} was found to be approximately 1000. For greater wavelengths, b_{ozone} was found to be even less. Thus, in the visible region, b_{ozone} is negligible compared to b_{scat}.

A similar comparison of b_{scat} to b_{NO_2} (b_{scat}/b_{NO_2}) was made by Charlson and Covert[11] in which b_{scat} was measured by an integrating nephelometer and b_{NO_2} was calculated from values of the NO_2 concentration and the absorption coefficient of NO_2. Figure II-1 is a

graph of the extinction coefficient due to scattering at .55μ versus the NO_2 concentration. Charlson and Covert have chosen the ratio of b_{scat}/b_{NO_2} equal to six to be that point at which b_{NO_2} is said to significantly contribute to the overall attenuation of light. At a b_{scat}/b_{NO_2} of twenty, scattering by aerosols is the dominating factor. The shaded-in area is the 90% confidence limit for the relation between mass and meteorological range.

Values of the light extinction coefficient of NO_2 have been measured.[12] Table II-1, Appendix, shows the value of the extinction coefficient of NO_2 for wavelengths in the visible range. It is seen that for the shorter wavelengths (blue and green) that b_{NO_2} has a more significant effect than in the longer visible wavelengths. The importance of b_{NO_2} to the overall extinction coefficient for the present work will be discussed in more detail in light of the results obtained. In the absence of NO_2, the attenuation of light in the visible, Equation II-10, reduces to

$$b = b_{Rayleigh} + b_{scat}. \qquad \text{(II-11)}$$

Noll and Pueschel[13] have examined the particle size frequency distribution of urban and maritime aerosols in order to determine those particles which attenuate light in the visible range. It was found that about 90% of the particles in an aerosol were smaller than .1μ. However, their total contribution to light extinction was found to be 5% at the most. The general absence of particles with radii greater than 1.0μ and the decrease in the scattering coefficient for particles smaller than .1μ lead to the conclusion that the size range of optical importance was limited to .1μ to 1.0μ.

Integrating Nephelometer

The evaluation of the visual quality of the air (extinction of light by particle scattering) has been aided by the adaptation

of the Brewer and Beuttell integrating nephelometer to measure air quality. The basic design of the nephelometer is discussed by Ahlquist and Charlson.[14,15] It has been successful in the following areas:[15]

1. studying the relationship between mass concentrations, light scattering, and visibility,
2. monitoring light scattering coefficient as a function of time at a stationary location,
3. measurement of the ratio of dispersion of smoke from the burning of logging wastes and forest aerosols,
4. mobile reconnaissance and the problems of spatial variation in urban areas,
5. studies of aerosol background in air entering the Pacific Northwest from uninhabited areas,
6. investigations of the wavelength dependence of the light scattering coefficient of atmospheric aerosol.

It has also been demonstrated that the integrating nephelometer can be used by single engine aircraft[16] to measure particulate or mass loading.

Veress[7,17] has shown that the Charlson-Ahlquist type of nephlometer can be used to evaluate smoke plumes by mounting the instrument in an airplane and flying through the plume at different distances downwind. A comparison between the values of the extinction coefficient as measured by the nephlometer was made with the values of the extinction coefficient determined by photogrammetry. Final conclusions of this comparison were not available at the printing of the article. It should be noted that the relation between density and scattering coefficient as derived by Veress[7] is not mathematically correct in that

$$\log\left(e^{-\sigma_s l}\right) = -\sigma_s l \neq e^{-\sigma_s l}.$$

Likewise, some of the equations derived by Veress[17] in a similar article are not mathematically correct in that

$$\log \frac{a}{b} = \log a - \log b \neq (\log a)/\log b.$$

The development of the relationship between photographic theory and light extinction, as used by Veress, will be discussed later in this report as it is quite similar and applies to the processes used herein.

Effect of Relative Humidity on Attenuation Coefficient

In using instruments that measure the light scattering properties of the atmosphere, Charlson and Ahlquist have suggested that a hygrometer be employed to measure the effect of humidity on the measured scattering coefficient. Charlson and Ahlquist[18] found that a significant increase in the scattering coefficient occurred above a relative humidity of about 70% due to the increased growth in the diameter of small particles. Pilat[19] has shown that this effect occurs for the hydrated sodium sulfate aerosol (Na_2SO_4-H_2O). In a similar report, Lundgren and Cooper[20] have studied laboratory and ambient aerosols, finding that, in some cases, effects of humidity occurred at relative humidities as low as 50%. However, it was found that if the relative humidity (R.H.) was lowered by drying the sample to 30% R. H. or below, then the sample could be compared to a dry aerosol.

The nephelometer developed by Charlson has a heater in its air stream which may or may not be used to lower the relative humidity to below 40%, depending on the type of measurements that are desired. This allows relative humidity effects to be minimized in this instrument.

CHAPTER III

THEORETICAL CONSIDERATIONS

I. PHOTOGRAPHY AND LIGHT INTENSITY

Bouguer-Lambert Law

The basic equation used is the Bouguer-Lambert extinction law. Assuming that scattering prevails over absorption, this law reduces to the well-known expression,

$$I_x = I_o \exp(-bX), \qquad \text{(III-1)}$$

where I_o is the initial intensity and I_x is the resultant intensity of radiation after passing through a distance, X, containing particles with an extinction coefficient, b. The scattering coefficient may be constant or a function of X.

Relation between Exposure, Density, and Intensity

Photography may be used to measure the intensities of reflecting targets. If unexposed film is exposed to an intensity, I, for a given time, t, then the exposure is

$$E = It. \qquad \text{(III-2)}$$

If the film is exposed to a series of different intensities, then the film response can be measured. Film exposure is related to the density, D, by the expression

$$D = \gamma \log E \qquad \text{(III-3)}$$

or

$$D = .434\gamma \ln E \qquad \text{(III-4)}$$

where gamma (γ) is the characteristic of the film; thus,

$$D = .434\ \gamma \ln It. \qquad \text{(III-5)}$$

Luminance of a Colored Object

In relating the density, D, of an object on photographic film to the actual intensity of the object, one must consider that the film is exposed in a camera through an objective. In Equation III-5, the quantity, I, must be replaced by the illuminance, I_f, in the focal plane of the camera. This illuminance is expressed by the following equation:[17]

$$I_f = \frac{B_o T_e}{4(f_\#)^2 F} , \qquad \text{(III-6)}$$

where T_e is the transmission of the camera lens, $(f_\#)$ is the relative aperture setting, F is the filter factor, and B_o is the luminance of the object as received at the camera lens. Thus, B_o is a combination of three components:

1. The first component is the reflected luminance from the target that is not scattered or absorbed by an aerosol layer between the target and distance, X. This can be written as $I_s R_g T_a$, where I_s is the incident illuminance of the object, R_g is the reflectance of the object in the direction of the camera, and T_a is the transmission of the atmosphere.
2. The second component is the luminance produced by the scattering of the sun's rays that penetrate the layer below the camera. (This is termed sky-light.)
3. The third component is the luminance produced by the sky, indirect sky-light. (This is termed diffuse light.)

The sky-light and diffuse light are expressed by the symbol, B_a, the total atmospheric illuminance. Figure III-1, Appendix, is an illustration of how these three components contribute to the total luminance, B_o, for colored (reflecting) and black (absorbing) targets. Therefore,

$$B_o = I_s R_g T_a + B_a . \qquad \text{(III-7)}$$

Substitution of this value of B_o and Equation III-6 into Equation III-5 yields the photographic density of an object:

$$D = .434\ \gamma_D \ln \left[\frac{(I_s R_g T_a + B_a) T_e t}{4(f_\#)^2 F}\right] , \qquad \text{(III-8)}$$

where I_s and B_a are in foot-candles. Converting to the meter-candle system, the general equation for the photographic density of an object becomes:

$$D = .434\ \gamma_D \ln \left[\frac{2.7\ (I_s R_g T_a + B_a) T_e t}{(f_\#)^2 F}\right] . \qquad \text{(III-9)}$$

Luminance of a Black Object

If the object in question is a perfect black body (totally absorbing) instead of a colored (wavelength-dependent reflection) object, then R_g is zero and Equation III-9 reduces to

$$D_B = .434\ \gamma_B \ln \left[\frac{2.7\ B_a T_e t}{(f_\#)^2 F}\right] , \qquad \text{(III-10)}$$

where D_B is the density of the black body as seen by the photographic film.

Relation between Density and Extinction Coefficient

Referring to Figure III-1, if the atmosphere is horizontally uniform, meaning that the extinction coefficient, b, is constant in the direction parallel to the earth's surface, then B_a has the same value at a point above a colored target that it does above a black target. This provides a very useful technique to correct the density of an object for sky-light and diffuse light. Rearranging Equations III-9 and III-10,

$$\frac{D}{.434\ \gamma_D} = \ln\left[\frac{2.7\ (I_s\ R_g\ T_a + B_a)\ T_e\ t}{(f_\#)^2\ F}\right] \qquad \text{(III-11)}$$

and

$$\frac{D_B}{.434\ \gamma_B} = \ln\left[\frac{2.7\ B_a\ T_e\ t}{(f_\#)^2\ F}\right] . \qquad \text{(III-12)}$$

Raising each equation to the exponential power of e, and subtracting Equation III-12 from Equation III-11, the resulting equation is that

$$e^{\frac{D}{.434\ \gamma_D}} - e^{\frac{D_B}{.434\ \gamma_B}} = \frac{2.7\ (I_s\ R_g\ T_a)\ T_e\ t}{(f_\#)^2\ F} ,$$

or

$$\ln\left[e^{\frac{D}{.434\ \gamma_D}} - e^{\frac{D_B}{.434\ \gamma_B}}\right] = \ln\left[\frac{2.7\ (I_s\ R_g\ T_a)\ T_e\ t}{(f_\#)^2\ F}\right] . \qquad \text{(III-13)}$$

Referring to Equation III-9, if the camera is at a distance such that scattering and absorption are negligible compared to the reflected intensity, then T_a approaches unity corresponding to one hundred percent transmittance of the object's reflected light. This occurs as X approaches zero. The quantity B_a also approaches zero under these conditions. Thus, for a camera very close to an object, Equation III-9 reduces to

$$D_o = .434\ \gamma_o \ln \frac{2.7\ (I_s\ R_g)\ T_e\ t}{(f_\#)^2\ F} , \qquad \text{(III-14)}$$

where D_o is the density of the object at zero distance. Subtracting Equation III-14 from Equation III-13,

$$\ln\left[e^{\frac{D}{.434\ \gamma_D}} - e^{\frac{D_B}{.434\ \gamma_B}}\right] - \frac{D_o}{.434\ \gamma_o} = \ln T_a . \qquad \text{(III-15)}$$

The transmission of a layer of air between zero distance and distance X is defined as

$$T_a = \frac{I}{I_o} = e^{-bX}. \qquad \text{(III-1)}$$

Substitution of this relation into Equation III-15 produces the final equation:

$$\ln \left[e^{\frac{D}{.434\ \gamma_D}} - e^{\frac{D_B}{.434\ \gamma_B}} \right] - \frac{D_o}{.434\ \gamma_o} = -bX. \qquad \text{(III-16)}$$

Equation III-16 is the theoretical working equation since it includes all the variables necessary to measure losses in intensity. By proper consideration of the densities of black and colored objects at various altitudes, this equation theoretically enables one to compare a loss or change in the density of an object (an indirect measure of the intensity) with variations in the atmospheric attenuation produced by an aerosol.

The importance of Equation III-16 is two-fold:

1. It provides a method to determine the accumulative bX between the ground and altitude, X, based on ground density data and aerial density data at the altitude in question. As a result, the average, b, can be determined.
2. For remote sensing of the environment, it provides a method through which aerial photographs of earth features can be corrected for the attenuation of light due to an aerosol layer, provided the coefficient of extinction of the layer is known.

II. INTERPRETATION OF THE PHOTOGRAPHIC CONSTANT

The γ-Curve

Equation III-16 is quite sensitive to the photographic constant, γ. As will be seen, γ is not necessarily constant, thus it is worthwhile to expound upon its meaning and interpretation. C. E. Mees, in The Theory of the Photographic Process - Chapter XIX,[20] has written a thorough explanation of the relation between density and exposure, namely,

$$D = \gamma \log E. \qquad \text{(III-3)}$$

The following discussion is taken primarily from that book. The most generally used curve for determining γ is the Hurter and Driffield characteristic curve (H and D curve). The general form of this curve for positive film can be seen in Figure III-2, Appendix, in which the various parts of the curve are labelled. The curve is constructed by exposing a photographic material to a known amount of radiation, developing the material, and then measuring the densities resulting from the various exposures. The results are expressed graphically by plotting the measured density against the logarithm of the exposure. For the straight line portion of this curve,

$$\gamma = \tan \alpha = \frac{dD}{d \log E} = \frac{\Delta D}{\Delta \log E} . \qquad \text{(III-17)}$$

However, this value of γ is only valid for density values ranging between points A and B in Figure III-2.

Shape of the γ-Curve

The shape of the characteristic curve depends on the conditions of development such as temperature, developing agent, and time of the development. Figure III-3, Appendix,[20] illustrates how the curve is shifted by increases in the time of development. Once the characteristic

curve has been established, then the exposure produced by any object can be determined provided the photographic material was developed under identical conditions.

For the case in which the measured density falls above point A or below point B in Figure III-2, γ is no longer constant, and varies as the density is changed. For these cases, it is necessary to take the instantaneous slope of the D-logE curve to determine γ. This is indicated by Equation III-17. Since it is no longer proper to call γ a constant, the measured γ corresponding to the density, D, is more properly labelled γ_D.

For a negative which is exposed to a series of different amounts of radiation, the characteristic curve is found in Figure III-4, Appendix.[20] The methods and techniques used for the positive print are equally applicable to the negative characteristic curve.

The Kodak Photographic Step Tablet

For simplicity in producing a characteristic curve, a semi-transparent density wedge is made by most photographic companies which consists of 21 densities running from densities of about .06 to 3.0.[21] Each step represents a density difference of about .15 or an actual exposure of 1.414 (the square root of two). By making a contact print of this photographic step tablet (Kodak Photographic Step Tablet No. 2) one can then obtain the characteristic curve of the negative by plotting the predetermined "original" densities of each step in the tablet as published by the manufacturer on the ordinate against the microdensitometer-measured densities on the abscissa. In this manner, γ_D can be determined for each measured density. This is illustrated in Figure III-5, Appendix.

Kodak Paper Gray Scale

A paper gray scale is also manufactured by Kodak which has 12 densities ranging from .06 to 1.74. This can be used instead of a step tablet to determine γ_D. A direct photograph is taken of this scale and the negative is analyzed to obtain the measured densities. A graph of the measured densities versus the original calibrated densities then allows one to obtain γ_D.

The Derivative of the D-LogE Curve

In using the D-LogE curve to determine γ_D, it is possible to obtain the derivative of the curve from which γ_D can be read directly as a function of the measured density. This becomes especially valuable if the characteristic curve is not straight over a wide range of densities. The curve illustrated in Figure III-6, Appendix, is the derivative of the γ-curve found in Figure III-5.

CHAPTER IV

EXPERIMENTAL APPARATUS AND PROCEDURE

I. MOBILE (AERIAL) APPARATUS

Integrating Nephelometer

A vertical profile of the scattering coefficient, b_{scat}, was made using an MRI integrating nephelometer Model No. 1550 and Recorder System No. 2050. This was accomplished by mounting the nephelometer and its recorder in an Aero Commander (Model 520, Serial #6, 1952) airplane. Figure IV-1, Appendix, is a diagram of the placement of the apparatus in the airplane. The scattering coefficient was recorded continuously on a revolving strip chart at a chart speed of one inch per minute. An event number was placed on the strip chart as each event was recorded. The system was powered by a portable battery system during some of the earlier experiments; however, due to the bulkiness of the battery system, an inverter was installed in the airplane's electrical system to convert the 24 volt d.c. system into a 110 volt a.c. system.

An illustrative diagram of the integrating nephelometer is shown in Figure IV-2, Appendix.[23] The measurement of the scattering of light is accomplished by a xenon flashlamp and a photomultiplier tube. With each flash of the lamp, the photomultiplier tube detects the light scattered from the particles in the sampling area. The current pulse from the photomultiplier tube is fed to an integrating circuit. At the same time, the current pulse from a reference phototube is fed into a similar circuit. The ratio of these two signals is amplified and passed through an RC network whose time

constant can be varied to regulate the averaging period of the measurements. This output is then amplified to a 5 volt full-scale level. The flashrate and averaging time are variable from 1/4-16 flashes per second and .1-200 seconds, respectively.

The MRI Instruction Manual--110A[23] suggests that for aircraft monitoring that a flashrate of 16 flashes per second and a time constant of .1 or 2 seconds be used. It was found that for the experimental set-up used, a flashrate of 16 flashes per second and a time constant of 2 seconds was suitable. For this time constant, the background noise of the output was approximately $\pm$ .05 b_{scat}, while for the .1 second time constant, the background noise was $\pm$ .15 b_{scat}.

Calibration of the Nephelometer

An absolute calibration of the nephelometer was done before each series of flights made. In cases where the nephelometer remained mounted in the aircraft for several days between flights, it was only necessary to perform a calibration check.

The calibration of the nephelometer is described in detail in the MRI Instruction Manual--110A. Basically, this consisted of calibrating two reference positions: the reference value of $.23 \times 10^{-4}$ meters^{-1} for $b_{Rayleigh}$ of pure air, and the value of 3.6×10^{-4} meters^{-1} for b_{scat} of Freon 12. This was accomplished by purging the system and filling the sampling chamber of the nephelometer with filtered air. This determined the clean air (background) reference point. Freon 12 was then introduced into the system and the second reference point was established. After checking these reference points and resetting the corresponding background and gain controls, the absolute calibration was complete. A reference calibration check is provided which allows a quick calibration check at any time during measurements.

Scattering Coefficient Measurements

A vertical profile of the scattering coefficient was obtained by measuring b_{scat} at each altitude that was flown. The accumulative bX, the right-hand side of Equation III-16, was determined by taking the total area under the X versus b_{scat} curve up to the altitude where the density, D, of the left-hand side of Equation III-16 was measured. This process whereby the area under the curve was obtained is illustrated in Figure IV-3, where the accumulative bX at four different altitudes (X_1, X_2, X_3, and X_4) is measured. The data from each vertical profile were treated in this manner.

Temperature Measurements

Dry-bulb (T_d) and wet-bulb (T_w) temperatures were measured by placing dry-bulb and wet-bulb thermometers in the air stream of the intake to the nephelometer. These were placed after the heater in the air stream so that the relative humidity of the sample could be determined just before it entered the nephelometer chamber. The thermometers were calibrated in degrees Fahrenheit (°F) with one division per degree. The accuracy of any individual reading was $\pm$ .5°F. Temperature readings, as well as the time, were recorded for each event which was recorded on the nephelometer.

Photographic Equipment

For photographic purposes, three Hasselblad Model 500EL/70 mm cameras were mounted in a 4-hole camera mount in the floor of the airplane. These were capable of taking 70 pictures in 65 seconds. Each camera contained one roll of Kodak Plus-X Aerocon 8401 (Estar Base) black and white film. The film is especially desirable for high-speed aerial photography at medium and high altitudes. A single synchronized electronic shutter release was used to insure that all three camera shutters operated in unison. Due to the manufacturer's

discontinuation of the production of the 8401 film, a similar film, Kodak Plus-X Aerographic 2402 (Estar Base) was used on some of the latter flights.

Each camera was equipped with a filter for selective sensitivity: one with a Hasselblad 3XG-1.5 green filter, one with a Hasselblad 2XCB6-1.0 blue filter, and one with a Hasselblad 6XR-2.5 red filter. In the latter flights, the blue filter was replaced by a Wratten #47 filter to obtain a narrower selective band pass. The spectral transmittance of each filter is shown in Figure IV-4, Appendix, for wavelengths ranging from .4μ to .7μ.

II. STATIONARY (GROUND) APPARATUS

Ground Targets

The objects photographed and analyzed in this investigation were four 20 feet by 20 feet targets: red, green, blue, and black. The red, green, and blue targets were purchased from Wright-Patterson Air Force Base. These were made of canvas and painted with special spectral reflective paint. See Figure IV-5, Appendix, for the spectral reflectance of each target as a function of wavelength. The black target was constructed of black felt, and backed with black plastic to minimize any reflection from its surface.

Other Ground Equipment

Other ground equipment consisted of:

1. one model 720 Gamma Scientific photometer with monochromator,
2. one Hasselblad Model 500EL/70 mm camera with interchangeable red, green, and blue filters identical to the aerial filters,

3. one Kodak Calibrated Paper Gray Scale (Serial No. 906GS213) with reflection densities ranging from .00 to 1.74 in 12 incremental steps (See Figure IV-6, Appendix),
4. one Kodak Step Tablet No. 2 (Serial No. 007ST471) with calibrated densities ranging from .06 to 3.00 in 21 increments,
5. one Voltz sun-photometer for turbidity and sun intensity measurements.

III. EXPERIMENTAL PROCEDURE

Aerial Procedure

Aerial data was taken over the 20 feet by 20 feet colored targets at various altitudes beginning at an altitude of approximately 500 feet above the ground level (AGL) or 1400 feet mean sea level (MSL). The altitude was increased in 300-500 feet intervals with each successive pass over the targets. See Figure IV-7 for a diagram of the flight pattern. The typical time elapsed from one pass to the next was approximately two minutes. A complete series of flights consisted of making flights from as low as possible to a point well above the haze layer. Twenty minutes to an hour was required for a complete series of passes, depending on the haze layer thickness and the prevailing weather conditions such as wind speed and cloud build-up. The general time of day of the flights was usually between 11:00 a.m. and 1:00 p.m. (EST). This time was chosen because the intensity of the sun during this period changes very little with sun angle. During earlier and later periods of the day, there is a considerable change in the period of an hour's time.

Photographs were taken of the four large targets with the Hasselblad cameras using the red, green, and blue filters at each altitude. At altitudes lower than 1000 feet above ground, it was impossible to press the shutter release at the instant that the airplane was directly above the targets. Occasionally, the target was missed at these low altitudes, and it was necessary to make a second pass. Since it was not possible to be sure if the target was in the frame, three flights were generally made at the lowest pass. The camera mount, itself, had a set of bubble-leveling indicators with adjustment levers to insure that the mount was always in the same plane as the targets.

Photographs were also taken of selective earth resource features such as forest-water interfaces, highway clover-leaf intersections, and an oil tank farm while making the circular return to the four target panels. Data were recorded above these in the same manner as above the four targets, with the exception of ground data. Analysis of these data was postponed until the completion of the analysis of the four colored targets.

Ground Procedure

On the ground, photographs of the targets were taken with the Hasselblad camera every four to ten minutes using the three filter combinations. The frame number and time were recorded in order that these might be compared to the aerial photographs taken at the same time. The ground photographs were all taken at a height of six feet directly above the targets. Care was taken to avoid any shadows on the targets.

The Kodak Calibrated Paper Gray Scale was placed on the black target and was photographed to determine γ. An analysis of the ground data showed that there was no measurable difference in the

γ-curve determined at three feet and the one determined at six feet. Thus, on all flights, a photograph was taken at three feet rather than at six feet to make the analysis of the negative easier. This same procedure was carried out for the red, green, and blue filters, respectively.

A photograph was also taken of the Kodak Step Tablet No. 2 which was taped to a piece of ground glass over a white reflecting panel. The ground glass was used to insure a uniform lighting of the step tablet. The negative of this photograph was analyzed to determine γ. Both the Kodak scales produced the same γ for each density measured. Figure IV-8, Appendix, is a graph showing the comparison between the curves for a ground experiment performed for the specific purpose of comparing the two scales. The γ-curve for the step tablet is shifted because it was backed by the ground glass; however, the slope of each curve (γ) is still the same. Thus, either method will produce the desired γ-curve.

IV. FILM ANALYSIS

Film Processing and Mounting

The film taken on the ground and in the air was developed at 72°C for four minutes and fifty-five seconds. Two rolls were developed at the same time. After the film was developed, the negatives were examined. The negatives of the aerial targets, the paper gray scales, and the ground targets were then cut out of the negatives, mounted on 4 inch by 5 inch index cards, and labelled.

Microdensitometer Analysis

An automatic magnetic tape recording microdensitometer and recorder, Tech/Ops Scandig Model 25 and Kennedy Model 3110 Digital Tape Recorder, were used to determine the transmission densities of

the targets on the film at each altitude. The densitometer uses an electro-optical rotating drum to obtain pictorial information from a film negative or transparency. The Scandig quantitatively measures optical densities from 0-3D through 256 levels with a resolution of .012D.[24] The sampling lattice along the axis and along the circumference of the drum is 25,50, and 100 microns.

The output of the microdensitometer is stored on eight channels of magnetic tape as successive binary numbers proportional to the optical density of the point sampled. This is then fed into a computer. The output is then printed on paper forming the image of the sample but with a density scale ranging from 0-256. Figure IV-9, Appendix, is a flow diagram for the processes involved in the film analysis. Figure IV-10, Appendix, is a photograph of the computer print-out showing some of the symbols used. Each symbol is representative of a density value. However, there are only 100 different symbols; each symbol represents a density range of 2.5 out of 256. This density range is then converted to the 0-3D range. Therefore, the overall resolution of the density measurements using this system is .03 out of 3, or 1%.

In analyzing the data and scanning large areas where spatial resolution was not important, a 100 micron lattice was sufficient. For flight altitudes of 4000-8000 feet it was necessary to use the 25 micron scanning lattice because of the decreasing size of the targets. The densities of the targets and step wedges were determined for each set of filters and placed in tabular form. Gamma (γ) was then determined for each of the filters for the data analyzed, as previously described.

CHAPTER V

EXPERIMENTAL RESULTS

I. DESCRIPTION OF FLIGHTS

Flights Made

Ten flights were made throughout the duration of the research effort. These were coded according to the date the flights were made:

1. August 11, 1971 Flight
2. August 19, 1971 Flight
3. October 12, 1971 Flight
4. October 26, 1971 Flight
5. October 28, 1971 Flight
6. June 30, 1972 Flight
7. July 12, 1972 Flight
8. July 20, 1972 Flight
9. July 24, 1972 Flight
10. November 6, 1972 Flight

Developmental Experiments of August 11 to October 26, 1971

The first four flights were primarily developmental flights which eventually led to the experimental procedure described in Chapter IV. These four flights provided useful information such as the profile of the scattering coefficient and the relative humidity in the vertical direction. However, the technique of employing a black (absorbing) target to distinguish between the targets reflected energy and the energy received at the camera from target, diffuse-, and sky-light was not used on these flights.

After these data were reviewed, it was determined that it was not possible to relate the scattering coefficient to changes in

densities above the targets without a more complex experimental procedure. Figure V-1, Appendix, is a graph of the change in density of the red, blue, and green targets for the August 10, 1971 flight. The photographs were taken with the Hasselblad red filter previously described. Included in Figure V-1 is a plot of the vertical profile of the scattering coefficient, b. A comparison of this graph with similar graphs of the data for the other three developmental flights did not provide any new information.

Experiment of October 28, 1971

This experiment was conducted in a similar manner to the previous four flights, but with the inclusion of a new particle counting instrument. The purpose of this flight was to compare the scattering coefficient as measured by the nephelometer with the particle count measured by a Bausch and Lomb particle counter (Model No. 40-1A). The particle counter was owned, operated, and calibrated by the Tennessee Valley Authority (TVA); it was flown in a TVA helicopter over the targets in conjunction with the airplane passes in which the nephelometer was used. It was not possible to convert the data from the two instruments to a common base. Thus, only a relative comparison was possible. Figure V-2, Appendix, is a graph of the vertical profiles of the scattering coefficient and the particle count on relative scales. It is seen that these two profiles are quite similar, indicating that the nephelometer yields results comparable to those obtained by the aerosol particle counter.

Flights of June 30 to November 6, 1972

After having analyzed the first five flights, it was determined that the target density data needed to be corrected for sky-light and diffuse light before any comparison could be made between

nephelometer-measured losses in intensity and photographically-measured intensity. A black (non-reflecting) target was introduced into the experimental procedure. The black target was included after the theory was developed for the complete relationship between density, altitude, and the scattering coefficient. The theoretical relationship, expressed as the following (Equation III-16):

$$\ln \left[e^{\frac{D}{.434\gamma_D}} - e^{\frac{D_B}{.434\gamma_B}} \right] - \frac{D_o}{.434\gamma_o} = -bX,$$

demonstrated the need for a black target to measure only sky-light and diffuse light.

The flights of June 30, July 12, July 20, July 24, and November 6, 1972, were all made with black targets and followed the experimental procedure outlined in Chapter IV. Table V-1, Appendix, shows each of these flights, describes the filter combinations used, and explains why certain data and filter combinations were not available for some of the flights. There was a malfunction in the synchronized shutter release in two of the cameras during three of these flights.

II. ANALYSIS OF THE FLIGHTS

Flights of June 30 to November 6, 1972

As a result of the experimental flights, five sets of data were found to be complete enough to allow evaluation. See Table V-1 for these flights and filter combinations. These data were analyzed for the following information:

1. the accumulative bX at each altitude from the nephelometer data (Figures V-3, V-4, and V-5, Appendix),
2. target densities at each altitude (Tables V-2, V-3, and V-4, Appendix),

3. relative humidity for each altitude (Figures V-3, V-4, and V-5, Appendix),
4. γ-curves for each flight (Figures V-6, V-7, V-8, Appendix),
5. γ for each measured density (Figures V-9, V-10, V-11, Appendix).

Assumption that $\gamma_B = \gamma_D$

Because of the form of the γ-curves (Figure V-6), it was found that the γ_B corresponding to the measured densities of the black target did not give useful results. This was a result of the rapid change in γ with density in this part of the curve. Because of this inability to use γ_B experimentally, the following assumption was made:

> Assumption--Assume that the γ corresponding to the density of the black target at a specific altitude, γ_B, is identical to the γ corresponding to the density of the colored target at the same altitude.

Applying this assumption to the theoretical equation, Equation III-16 then becomes the following:

$$\ln \left[e^{\frac{D}{.434\gamma_D}} - e^{\frac{D_B}{.434\gamma_D}} \right] - \frac{D_o}{.434\gamma_o} = -bX. \qquad \text{(V-1)}$$

Application of Equation V-1 to the Experimental Data

Equation V-1 was applied to all the information from the five complete sets of data (Table V-1). Calculations were made of the photographically-determined values of bX. These are included in Tables V-2, V-3, and V-4, along with the bX values determined by the nephelometer.

Dependence of $|\Delta bX|$ on $|\Delta\gamma/\Delta D|$

Figure V-12 is a plot of the absolute value of the difference between the photographically-determined bX and the nephelometer-

determined bX ($|\Delta bX|$) against $|\Delta\gamma/\Delta D|$. From this graph it is seen clearly that for $|\Delta\gamma/\Delta D| > 1.0$, there is a significant increase in $|\Delta bX|$. See back-up Figures V-9, V-10, and V-11.

This can be explained by realizing that the measured density versus calibrated density curve (Figures V-6, V-7, and V-8) from which γ was determined, was constructed from 12 data points. For densities which did not fall at these values, it was necessary to interpolate by constructing a smooth curve through the points. When γ is changing rapidly (the second derivative of the measured density versus the calibrated density is unequal to zero), then it becomes increasingly more difficult to determine the instantaneous γ with any accuracy. The result is that for values of $|\Delta\gamma/\Delta D| > 1.0$, the value of bX can not be determined.

Limitations on the Experiment as a Result of $|\Delta\gamma/\Delta D|$

Figure V-12 shows that for values of $|\Delta\gamma/\Delta D| > 1.0$, the accuracy of measurement of bX by photographic means decreases rapidly. For $|\Delta\gamma/\Delta D| \lesssim 1.0$, bX can be determined within a value of bX $\pm$ .05. Furthermore, it is seen in this figure that the accuracy does not improve for $|\Delta\gamma/\Delta D| \leq 1.0$. Figure V-16, Appendix, is a graph of all the data taken for which $|\Delta\gamma/\Delta D| \leq 1.0$. A least square analysis was run on this data and is illustrated in the figure.

It is seen from Table V-2, V-3, and V-4, that the limitation of $|\Delta\gamma/\Delta D| \leq 1.0$ has eliminated all of the filter-target combinations except for red filter-red target and blue filter-blue target. This should not be interpreted to mean that the other filter combinations will not produce significant results. For the remaining filter combinations there is the possibility of developing the film for a longer or shorter time period to try to lower the value of $|\Delta\gamma/\Delta D|$ below 1.0. From Figure III-3, Appendix, it can be seen that the γ-curve can be changed by varying the time of development. Since

the accuracy of the experiment is dependent on the rate of change of γ with the density, it should be possible to produce a negative with $|\Delta\gamma/\Delta D| \leq 1.0$ for most filter combinations. The regions in which $|\Delta\gamma/\Delta D| \leq 1.0$ (the useable regions) are labelled by points C and D in Figures V-6, V-7, and V-8.

Relative Humidity and NO_2 Effects

A vertical profile of the relative humidity was determined for each flight as described in Chapter IV. These proviles are included in Figures V-3, V-4, and V-5, Appendix. The relative humidity was found to be less than 65% on all flights made; thus it can be concluded that its effect on the nephelometer-measured values of bX was negligible.

The effect of absorption by NO_2 on the attenuation coefficient was estimated to be at most 5-10% based on typical values of the NO_2 concentration in the Knoxville, Tennessee area.

Summary

Although much work is still needed in this research area, it has been shown by this effort that it is possible to measure the accumulative bX by the photographic process using the developed theoretical equation, Equation III-16. Necessary conditions to obtain meaningful measurements are that

1. $\gamma_B = \gamma_D$
2. $|\Delta\gamma/\Delta D| \lesssim 1.0$.

With these two conditions, bX has been measured with an accuracy of bX $\pm$ .05. For the average aerosol concentrations in the Knoxville, Tennessee area of 68 $\mu g/m^3$ particulate matter[25] (2.3×10^{-4} m^{-1} = b_{scat}), this represents an error of approximately $\pm$ 22% for an air layer of 1000 meters. However, on days in which high particulate

air pollution levels exist ($4\text{-}5 \times 10^{-4}\ m^{-1} = b_{scat}$), the error in this method is reduced to $\pm$ 10%.

This research effort has demonstrated that it is possible to determine the amount of particulate air pollution present between a target and the altitude of an aerial photograph by application of a theoretically developed equation. The required parameters to solve the theoretical equation are as follows:

1. reflected film density at ground,
2. reflected film density at flight altitude,
3. density of a black target as seen at flight altitude.

CHAPTER VI

FUTURE RESEARCH

There are several important areas in which this research effort may be extended. Additional research is needed to evaluate the possibilities of using any number of different filter-target color combinations to allow a more versatile application of the procedure. Ground experiments can be done to see if it is possible to produce γ-curves for which $|\Delta\gamma/\Delta D| \leq 1.0$ for many different filter combinations.

This research effort can also be extended into the area of remote sensing of the environment by earth satellites. By having ground-based knowledge of how the density of appropriate earth features change with incoming intensity of the sun's radiation, it should be possible to relate the change in this ground-based density, as seen by a satellite, to changes in average scattering coefficient, $\bar{b}$, of the atmosphere. Because of the large extent of ground coverage by satellite sensing, this provides a means for large-scale (state and regional) mapping of particulate air pollution without the use of an extensive ground-based monitoring system. In like manner, earth features which change with the seasons of the year such as vegetation can be evaluated more accurately by remote sensing. By first evaluating a region using seasonally-unchanging earth features and mapping the particulate air pollution, it would then be possible to evaluate seasonally-changing features for changes in density produced by the overlying aerosol. This would allow correction of the day to day variations of the density of an earth feature as seen by a satellite and allow a more accurate evaluation of the environment by remote sensing techniques.

This research effort might also be extended into remote sensing in the infrared provided an equivalent "black" target could be found in this spectral region.

LIST OF REFERENCES

LIST OF REFERENCES

1. Duntley, Seibert Q. "Visibility," Applied Optics, Vol. 3, No. 5, May, 1964, pp. 549-556.

2. Duntley, Seibert Q. "The Reduction of Apparent Contrast by the Atmosphere," Journal of the Optical Society of America, Vol. 38, No. 2, February, 1948, pp. 179-190.

3. Mazurowski, Melvin J. and Roger D. Sink. "Attenuation of Photographic Contrast by the Atmosphere," Journal of the Optical Society of America, Vol. 55, No. 1, January, 1965, pp. 26-30.

4. Coleman, Howard S., Fred J. Morris, Harold E. Rosenberger, and Marshall J. Walker. "A Photoelectric Method of Measuring the Atmospheric Attenuation of Brightness Contrast Along a Horizontal Path for the Visible Region of the Spectrum," Journal of the Optical Society of America, Vol. 39, No. 7, July, 1949, pp. 515-521.

5. Coleman, Howard S. and Harold E. Rosenberger. "A Comparison of Photographic and Photoelectric Measurements of Atmospheric Attenuation of Brightness Contrast," Journal of the Optical Society of America, Vol. 39, No. 12, December, 1949, pp. 990-993.

6. Conner, William D. Optical Properties and Visual Effects of Smoke-Stack Plumes, U. S. Department of Health, Education, and Welfare. Public Health Service No. 999-AP-30.

7. Veress, S. A. "Air Pollution Research," Photogrammetric Engineering, Vol. 36, 1970, pp. 840-848.

8. Charlson, Robert J., Norman C. Ahlquist, and Helmuth Horvath. "On the Generality of Correlation of Atmospheric Aerosol Mass Concentration and Light Scatter," Atmospheric Environment, Vol. 2, 1968, pp. 455-464.

9. Moller, F. "Optics of the Lower Atmosphere," Applied Optics, Vol. 3, No. 2, February, 1964, pp. 157-166.

10. Elterman, L. "Rayleigh and Extinction Coefficients to 50 km for the Region 0.27μ to 0.55μ," Applied Optics, Vol. 3, No. 10, October, 1964, pp. 1139-1147.

11. Charlson, R. J., D. S. Covert, Yoshiro Tokiwa, and Peter Mueller. "Multiwavelength Nephelometer Measurements in Los Angeles Smog Aerosol III: Comparison to Light Extinction by NO_2," University of Washington.

12. The Oxides of Nitrogen in Air Pollution. Department of Public Health, State of California, Berkeley, California, January, 1966, pp. 53-63.

13. Pueschel, Rudolf F. and Kenneth E. Noll. "Visibility and Aerosol Size Frequency Distribution," Journal of Applied Meteorology, Vol. 6, No. 6, December, 1967, pp. 1045-1052.

14. Ahlquist, Norman C. and Robert J. Charlson. "A New Instrument for Evaluating the Visual Quality of Air." Pacific Northwest International Section of the Air Pollution Control Association Meeting, Seattle, Washington, November, 1966.

15. Charlson, Robert J. "Atmospheric Aerosol Research at the University of Washington," Journal of the Air Pollution Control Association, Vol. 18, No. 10, pp. 652-654, October, 1968.

16. Adams, D. F. and R. K. Koppe. "Instrumenting Light Aircraft for Air Pollution Research," Journal of the Air Pollution Control Association, Vol. 19, No. 6, pp. 410-415, June, 1969.

17. Veress, S. A. "Study of the Three Dimensional Extension of Polluted Air," Final Technical Report, Public Health Service Contract AP-00661-01.

18. Ahlquist, Norman C. and Robert J. Charlson. "Measurement of the Vertical and Horizontal Profile of Aerosol Concentration in Urban Air with the Integrating Nephelometer," Environmental Science and Technology, Vol. 2, No. 5, May, 1968, pp. 363-366.

19. Pilat, Michael J. "Effects of Sorption on the Size Distribution and Optical Properties of an Aerosol." Pacific Northwest International Section of the Air Pollution Control Association Meeting, Seattle, Washington, November, 1966.

20. Lundgren, D. A. and D. W. Cooper. "Effects of Humidity on Light-Scattering Methods of Measuring Particle Concentration," Journal of the Air Pollution Control Association, Vol. 19, No. 4, April, 1969, pp. 243-247.

21. Mees, C. E. Kenneth. The Theory of the Photographic Process. The Macmillan Company, New York, 1944, pp. 699-751.

22. "Kodak Notes on Practical Densitometry," Pamphlet E-S9.

23. Instruction Manual--110A, Meteorology Research, Inc., Altadena, California, July, 1970.

24. "University of Tennessee Microdensitometer Use and Description," Civil Engineering Department, The University of Tennessee College of Engineering, Knoxville, Tennessee.

25. Duncan, Joe R. and Terry Miller. Air Resource Management in Knox County: Technical Report No. 3, Knox County Department of Air Pollution Control, Knoxville, Tennessee, April, 1972.

26. Ahlquist, N. C. and R. J. Charlson. "Measurement of the Wavelength Dependence of Atmospheric Extinction Due to Scatter," Pacific Northwest International Section of the Air Pollution Control Association Meeting, Vancouver, British Columbia, Canada, November, 1968.

27. Charlson, R. J., N. C. Ahlquist, and H. Selvidge. "The Use of the Intergrating Nephelometer for Monitoring Particulate Pollution," Tenth Annual Conference on Methods in Air Pollution and Industrial Hygiene Studies, San Francisco, California, February, 1969.

28. Coleman, Howard S. and Harold E. Rosenberger. "The Attenuation of Brightness Contrast Caused by Atmospheric Optical Haze," Journal of the Optical Society of America, Vol. 40, No. 8, August, 1950, pp. 507-508.

29. Coulson, Kinsell L. "Effects of Reflection Properties of Natural Surfaces in Aerial Reconnaissance," Applied Optics, Vol. 5, No. 6, June, 1966, pp. 905-917.

30. Duntley, Seibert Q. "The Visibility of Distant Objects," Journal of the Optical Society of America, Vol. 38, No. 3, March, 1948, pp. 237-249.

31. Green, A. E. S., A. Deepak, and B. J. Lipofsky. "Interpretation of the Sun's Aureole Based on Atmospheric Aerosol Models," Applied Optics, Vol. 10, No. 6, June, 1971, pp. 1263-1279.

32. Green, A. E. S., A. Deepak, T. Sawada, and R. S. Sholtes. "Remote Sensing of Atmospheric Aerosols," Proceedings of the Seventh International Symposium on Remote Sensing of Environment, Vol. III, May 17-21, 1971, pp. 1749-1763.

33. Harris, William H. "Aerial Photographic Exposure," Manual of Color Aerial Photography, American Society of Photogrammetry, 1968.

34. Hochreiter, Frederick C. Analysis of Visibility Observation Methods, Technical Memorandum WBTM T & EL 9, Department of Commerce, Environmental Science Services Administration, Sterling, Virginia, October, 1969.

35. Horvath, Helmuth and Kenneth E. Noll. "The Relationship Between Atmospheric Light Scattering Coefficient and Visibility," Atmospheric Environment, Vol. 3, 1969, Peragamon Press, pp. 543-552.

36. Houghton, H. G. "The Transmission of Visible Light Through Fog," Physical Review, Vol. 38, July 1, 1931, pp. 152-158.

37. Idso, Sherwood B. "Seasonal Changes in the Vertical Distribution of Dust in the Lower Troposphere," Journal of Geophysical Research, Vol. 75, No. 12, April 20, 1970, pp. 2179-2185.

38. Irvine, William M. and Floyd W. Peterson. "Observations of Atmospheric Extinction from 0,315 to 1.06 Microns," Journal of the Atmospheric Sciences, Vol. 27, January, 1970, pp. 62-69.

39. Noll, Kenneth E., Peter K. Mueller, and Miles Imada. "Visibility and Aerosol Concentration in Urban Air," Atmospheric Environment, Vol. 2, Pergamon Press, pp. 465-475.

40. Marggraf, W. A. and M. Griggs. "Aircraft Measurements and Calculations of the Total Downward Flux of Solar Radiation as a Function of Altitude," Journal of the Atmospheric Sciences, Vol. 26, pp. 469-477.

41. Middleton, W. E. Knowles. Vision Through the Atmosphere. University of Toronto Press, 1952.

42. Porch, William M., Robert J. Charlson, and Lawrence F. Radke. "Atmospheric Aerosol: Does a Background Level Exist?" Science, Vol. 170, pp. 315-317.

43. Rosen, James M. "The Vertical Distribution of Particulate Matter Near the Surface of the Earth," Journal of the Air Pollution Control Association, Vol. 19, No. 2, February, 1969, pp. 106-108.

44. Turner, R. E., W. A. Malila, and R. F. Nalepka. "Importance of Atmospheric Scattering in Remote Sensing, or Everything You've Always Wanted to Know About Atmospheric Scattering But Were Afraid to Ask," Proceedings of the Seventh International Symposium on Remote Sensing of Environment, Vol. III, May 17-21, 1971, pp. 1651-1697.

45. Waldram, J. M. "Measurement of the Photometric Properties of the Upper Atmosphere," Quarterly Journal of the Royal Meteorological Society, Vol. 71, 1945, pp. 319-336.

APPENDIX

Table II-1. Values of the Light Extinction Coefficient of NO_2.

Wavelength, °A	b_{NO_2} ($PPM^{-1}Mile^{-1}$)	b_{NO_2} ($PPM^{-1}Mile^{-1}$)
4000	2.60	1.64
4500	2.07	1.31
5000	1.05	0.66
5500	0.47	0.30
6000	0.18	0.12
6500	.062	0.039
7000	.026	0.016

Sources: Computed from the Summary in "Photochemistry of Air Pollution," Philip A. Leighton, Academic Press, 1961.

The Oxides of Nitrogen in Air Pollution. Department of Public Health, State of California, Berkeley, California, January, 1966, pp. 53-63.

Table V-1. Type of Data Taken on Each Flight.

Flight	Filters Used on Targets	Aerial Data Available	Ground Data Available	Data Complete	Explanation
June 30, 1972	Red filter Green filter Blue filter	X X X	X X	X X	A second blue filter for the ground data was not available
July 12, 1972	Red filter Green filter Blue filter	X X X	X	X	No γ-curve for the green filter A second blue filter for the ground data was not available
July 20, 1972	Red filter Green filter Blue filter	X	X X		Malfunction in two aerial cameras A second blue filter for the ground data was not available
July 24, 1972	Red filter Green filter Blue filter	X X			Malfunction in the camera for the red filter and the ground data
November 6, 1972	Red filter Green filter Blue filter	X X X	X X	X X	No γ-curve for the green filter

Table V-2. Data for the June 30, 1972 Flight.

Filter	Target	Altitude	Density	Black Target Density	γ_0	γ_D	Calculated bX	Measured bX	ΔbX	$\frac{\Delta\gamma}{\Delta D}$
Red	Red	0	1.499	-	1.230	-	-	-	-	.78
Red	Red	105	1.342	.164	-	1.105	.099	.0189	.0801	.78
Red	Red	336	1.386	.257	-	1.140	.114	.0592	.0548	.78
Red	Red	458	1.289	.323	-	1.067	.157	.0805	.0765	.78
Red	Red	763	1.208	.323	-	.997	.155	.1350	.0200	.78
Red	Red	916	1.203	.396	-	.994	.187	.1630	.0240	.78
Red	Green	0	.633	-	.395	-	-	-	-	1.30
Red	Green	105	.515	.164	-	.36	.507	.0189	.488	1.30
Red	Green	336	.552	.257	-	.36	.323	.0592	.264	1.30
Red	Green	458	.558	.323	-	.36	.372	.0805	.292	1.30
Red	Green	916	.591	.396	-	.36	.249	.1630	.086	1.30
Red	Blue	0	.566	-	.36	-	-	-	-	1.30
Red	Blue	916	.528	.396	-	.36	.805	.1630	.642	1.30
Green	Green	0	1.016	-	.782	-	-	-	-	1.34
Green	Green	105	1.073	.247	-	.775	-.102	.0189	-.083	1.34
Green	Green	336	1.296	.616	-	.995	.225	.0592	.166	1.20
Green	Green	458	1.034	.456	-	.798	.217	.0805	.137	1.34
Green	Green	611	1.069	.541	-	.840	.330	.1080	.222	1.34
Green	Green	763	.993	.503	-	.776	.311	.1350	.176	1.35
Green	Green	916	1.000	.536	-	.772	.297	.1630	.135	1.34
Green	Red	0	.903	-	.633	-	-	-	-	2.00
Green	Red	105	.908	.247	-	.640	.115	.0189	.096	2.10
Green	Red	336	1.197	.616	-	.935	.610	.0592	.551	1.39
Green	Red	458	.920	.456	-	.664	.318	.0805	.238	1.90
Green	Red	611	.972	.541	-	.746	.592	.1080	.484	1.50
Green	Red	763	.892	.503	-	.615	.210	.1350	.075	2.00
Green	Red	916	.916	.536	-	.655	.370	.1630	.208	1.90

Table V-3. Data for the July 12, 1972 Flight.

Filter	Target	Altitude	Density	Black Target Density	γ_0	γ_D	Calculated bX	Measured bX	ΔbX	$\frac{\Delta\gamma}{\Delta D}$
Red	Red	0	1.546	-	1.10	-	-	-	-	0.0
Red	Red	61	1.546	.238	-	1.10	.0595	.021	.0385	0.0
Red	Red	183	1.572	.290	-	1.10	.0166	.066	-.0494	0.0
Red	Red	274	1.559	.341	-	1.10	.054	.100	-.046	0.0
Red	Red	412	1.509	.421	-	1.10	.185	.147	.038	0.0
Red	Red	427	1.514	.436	-	1.10	.177	.152	.025	0.0
Red	Red	641	1.489	.482	-	1.10	.249	.185	.064	0.0
Red	Red	732	1.516	.483	-	1.10	.185	.192	-.007	0.0
Red	Green	0	.611	-	.49	-	-	-	-	1.58
Red	Green	61	.607	.238	-	.485	.180	.021	.159	1.58
Red	Green	183	.638	.290	-	.540	.408	.066	.342	1.58
Red	Green	274	.681	.341	-	.610	.625	.100	.525	1.58
Red	Green	412	.709	.421	-	.650	.807	.147	.660	1.50
Red	Green	427	.728	.436	-	.705	.980	.152	.828	1.30
Red	Green	732	.746	.483	-	.74	1.13	.192	.938	1.20
Red	Blue	0	.499	-	.365	-	-	-	-	.70
Red	Blue	61	.514	.238	-	.375	.195	.021	.174	.73
Red	Blue	183	.539	.290	-	.396	.282	.066	.216	.90
Red	Blue	274	.602	.341	-	.477	.576	.100	.476	1.58
Red	Blue	412	.630	.421	-	.525	.896	.148	.749	1.58
Red	Blue	427	.635	.436	-	.535	.968	.152	.816	1.58
Red	Blue	641	.654	.482	-	.567	1.180	.185	.995	1.58
Red	Blue	732	.662	.483	-	.580	1.190	.192	.998	1.58

Table V-4. Data for the November 6, 1972 Flight.

Filter	Target	Altitude	Density	Black Target Density	γ_0	γ_D	Calculated bX	Measured bX	ΔbX	$\frac{\Delta\gamma}{\Delta D}$
Red	Red	0	.937	-	.865	-	-	-	-	0.79
Red	Red	397	.956	.106	-	.880	.107	.0436	.0634	0.80
Red	Red	550	.972	.108	-	.897	.115	.0604	.0546	1.02
Red	Red	641	1.007	.124	-	.935	.135	.0704	.0646	1.45
Red	Red	702	.962	.115	-	.886	.112	.0768	.0352	0.91
Red	Red	793	.973	.127	-	.900	.127	.0843	.0437	1.02
Red	Red	854	.957	.127	-	.883	.121	.0881	.0329	0.89
Red	Red	1053	.937	.131	-	.865	.125	.0985	.0265	0.79
Red	Red	1190	.949	.151	-	.873	.122	.1040	.0180	0.85
Red	Red	1250	.940	.144	-	.867	.127	.1070	.020	0.82
Red	Red	1390	.961	.162	-	.885	.128	.1120	.016	0.92
Red	Red	1465	.961	.164	-	.885	.129	.1150	.014	0.92
Red	Red	1558	.952	.164	-	.877	.130	.1180	.012	0.86
Red	Red	1770	.962	.166	-	.886	.130	.1250	.005	0.93
Red	Red	1860	.986	.210	-	.914	.163	.1270	.036	1.20
Red	Red	2105	.986	.184	-	.914	.153	.1330	.020	1.20
Red	Red	2470	.966	.193	-	.891	.143	.1410	.002	0.94
Red	Green	0	.318	-	.39	-	-	-	-	1.84
Red	Green	397	.252	.106	-	.22	-.514	.0436	-.558	3.40
Red	Green	550	.273	.108	-	.29	.025	.0604	-.040	2.48
Red	Green	641	.314	.134	-	.38	.286	.0704	.216	1.92
Red	Green	702	.275	.119	-	.30	.135	.0768	.058	2.40
Red	Green	793	.305	.127	-	.36	.313	.0843	.229	1.94
Red	Green	854	.297	.127	-	.35	.319	.0881	.231	1.98
Red	Green	1053	.288	.131	-	.33	.275	.0985	.177	2.04
Red	Green	1190	.316	.151	-	.38	.422	.104	.318	1.84

Table V-4. Data for the November 6, 1972 Flight (Cont.).

Filter	Target	Altitude	Density	Black Target Density	γ_0	γ_D	Calculated bX	Measured bX	ΔbX	$\frac{\Delta\gamma}{\Delta D}$
Red	Green	1250	.303	.144	-	.37	.457	.107	.350	1.94
Red	Green	1390	.320	.162	-	.39	.489	.112	.377	1.82
Red	Green	1465	.328	.164	-	.41	.544	.115	.429	1.76
Red	Green	1558	.322	.164	-	.40	.540	.118	.422	1.82
Red	Green	1770	.333	.166	-	.42	.564	.125	.439	1.72
Red	Green	1860	.363	.210	-	.46	.686	.127	.559	1.52
Red	Green	2105	.355	.184	-	.45	.601	.133	.468	1.56
Red	Green	2470	.357	.193	-	.46	.670	.141	.529	1.56
Blue	Blue	0	.484	-	.55	-	-	-	-	0.65
Blue	Blue	397	.529	.110	-	.570	.093	.0436	.049	.61
Blue	Blue	550	.548	.125	-	.580	-.024	.0604	.004	.59
Blue	Blue	641	.551	.144	-	.583	.074	.0704	.004	.58
Blue	Blue	702	.578	.154	-	.605	.049	.0768	-.029	.52
Blue	Blue	793	.587	.170	-	.610	.043	.0843	-.041	.48
Blue	Blue	854	.578	.168	-	.605	.063	.0881	-.025	.52
Blue	Blue	1053	.537	.172	-	.575	.140	.0985	.041	.60
Blue	Blue	1190	.568	.187	-	.598	.102	.104	-.002	.54
Blue	Blue	1250	.570	.193	-	.60	.107	.107	.000	.54
Blue	Blue	1390	.554	.198	-	.586	.133	.112	.021	.58
Blue	Blue	1465	.585	.216	-	.607	.091	.115	-.024	.50
Blue	Blue	1558	.580	.209	-	.605	.099	.118	-.019	.51
Blue	Blue	1770	.580	.212	-	.605	.102	.125	-.023	.51
Blue	Blue	1860	.563	.216	-	.592	.137	.127	.010	.56
Blue	Blue	2105	.575	.231	-	.602	.140	.133	.007	.53
Blue	Blue	2470	.601	.253	-	.616	.098	.141	-.043	.43

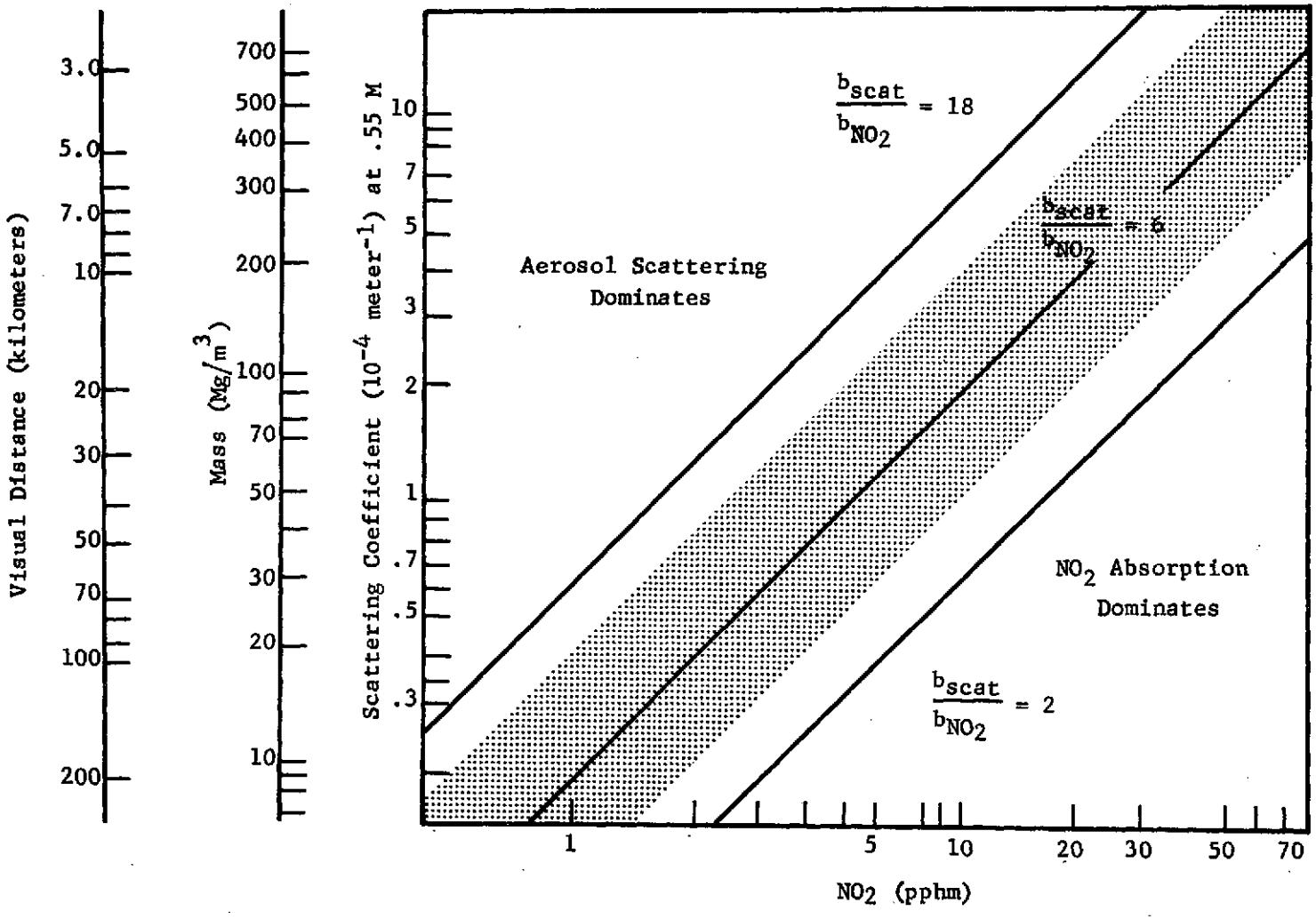

FIGURE II-1. Graph of b_{scat} Versus b_{NO_2}.

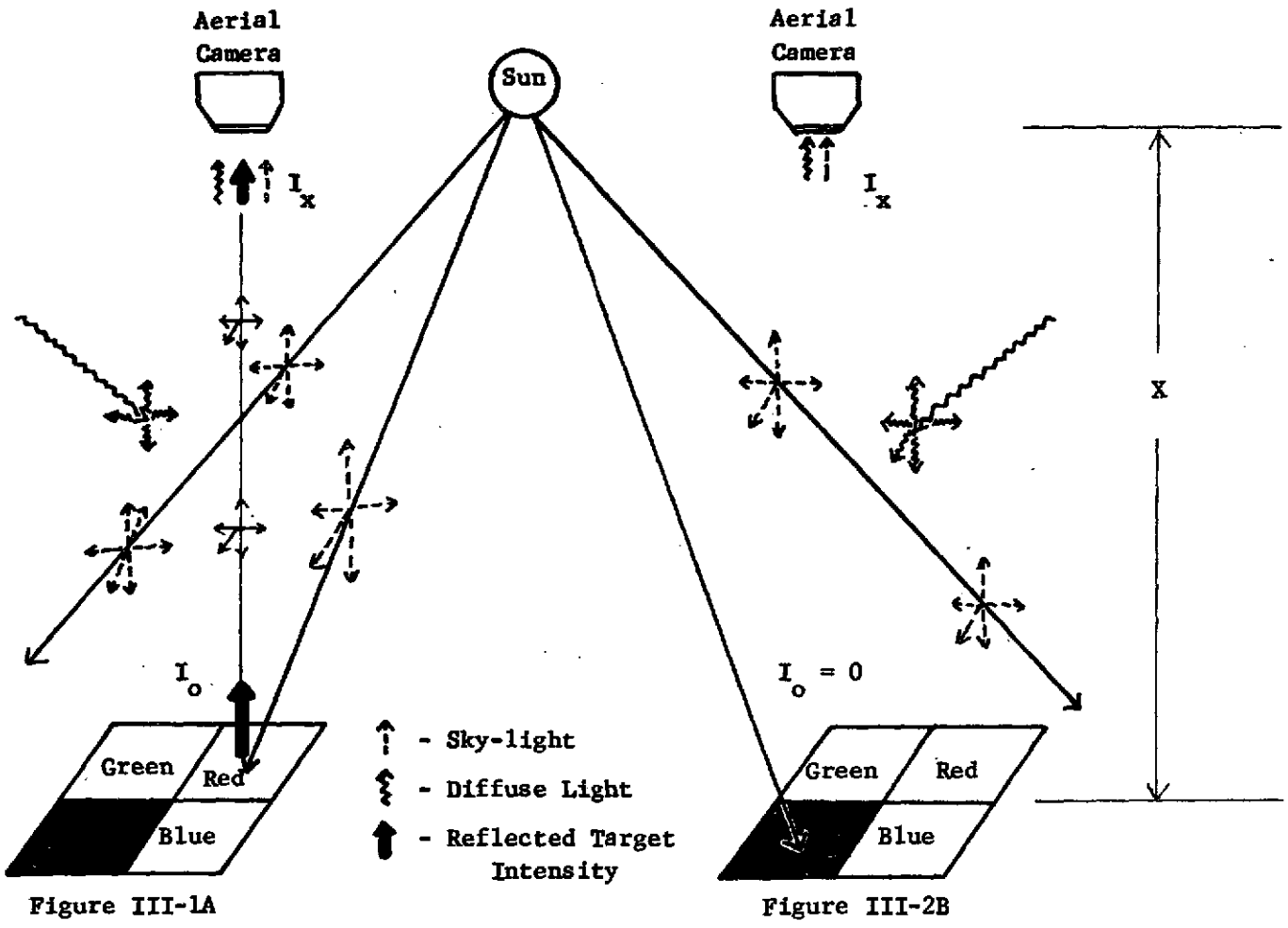

FIGURE III-1. Diagram of the Intensity Received by Aerial Camera from (A) a Colored Target, (B) a Black Target.

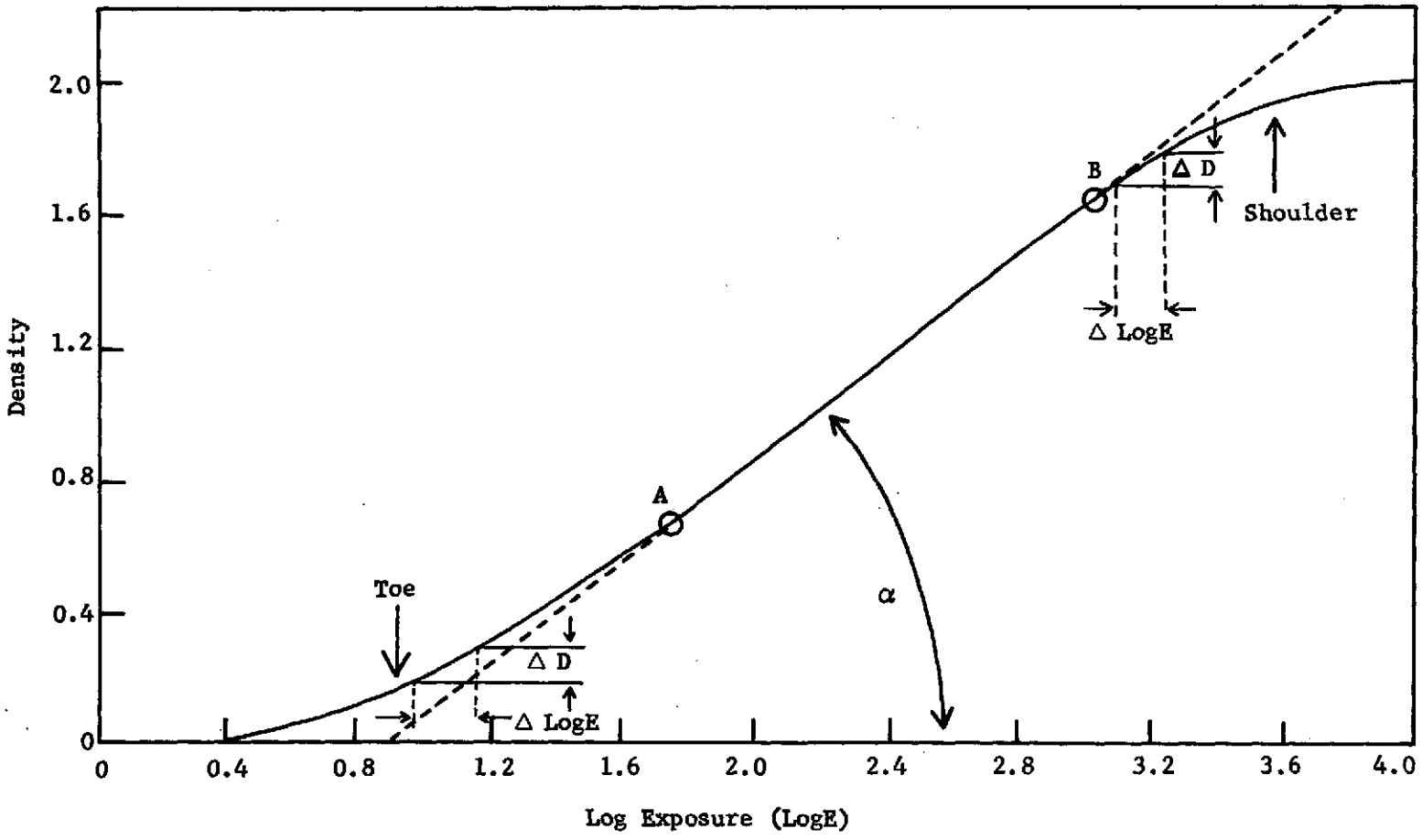

FIGURE III-2. The General Form of the γ-Curve for Positive Film.

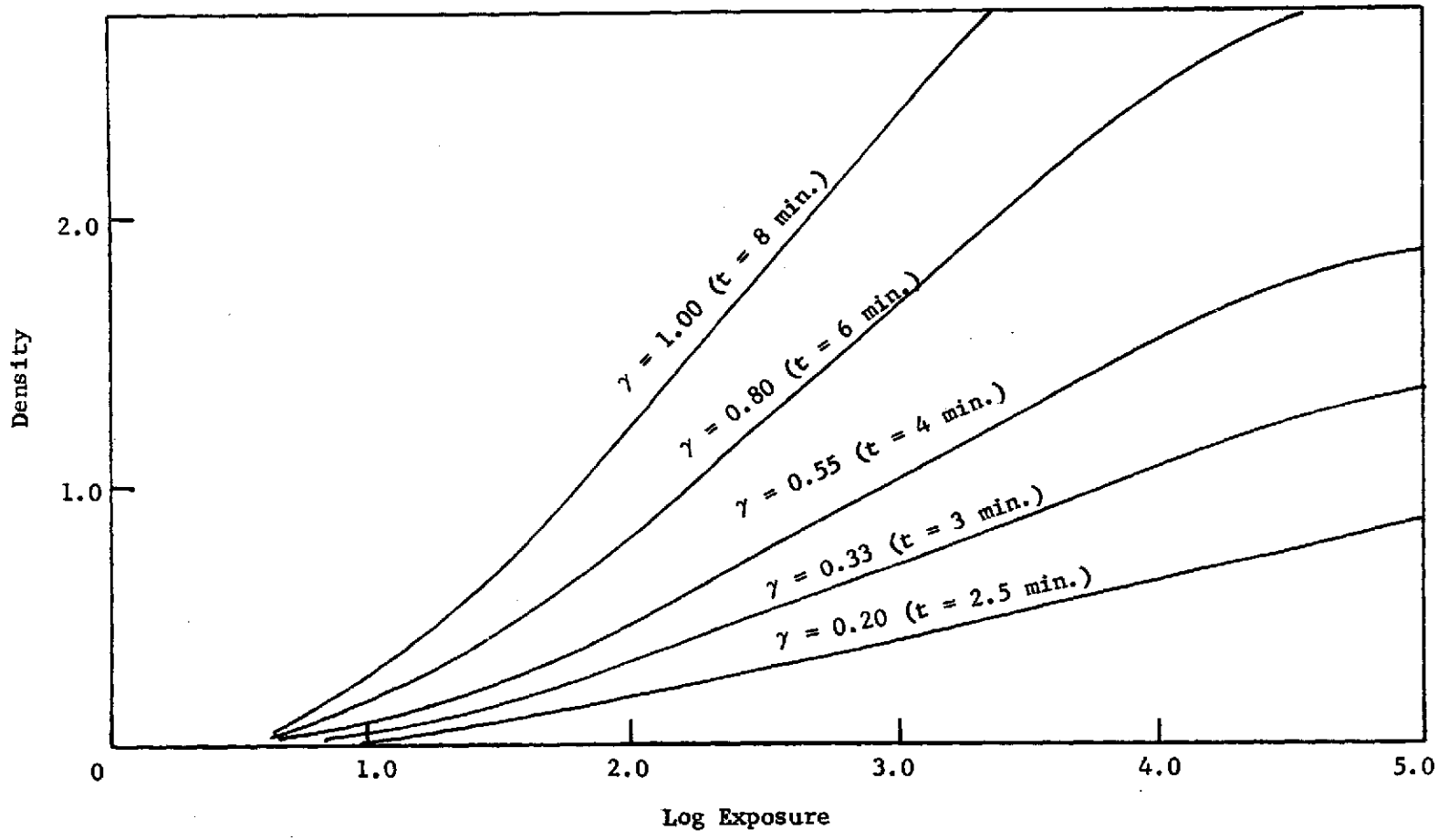

FIGURE III-3. The γ-Curve as a Function of the Development Time.

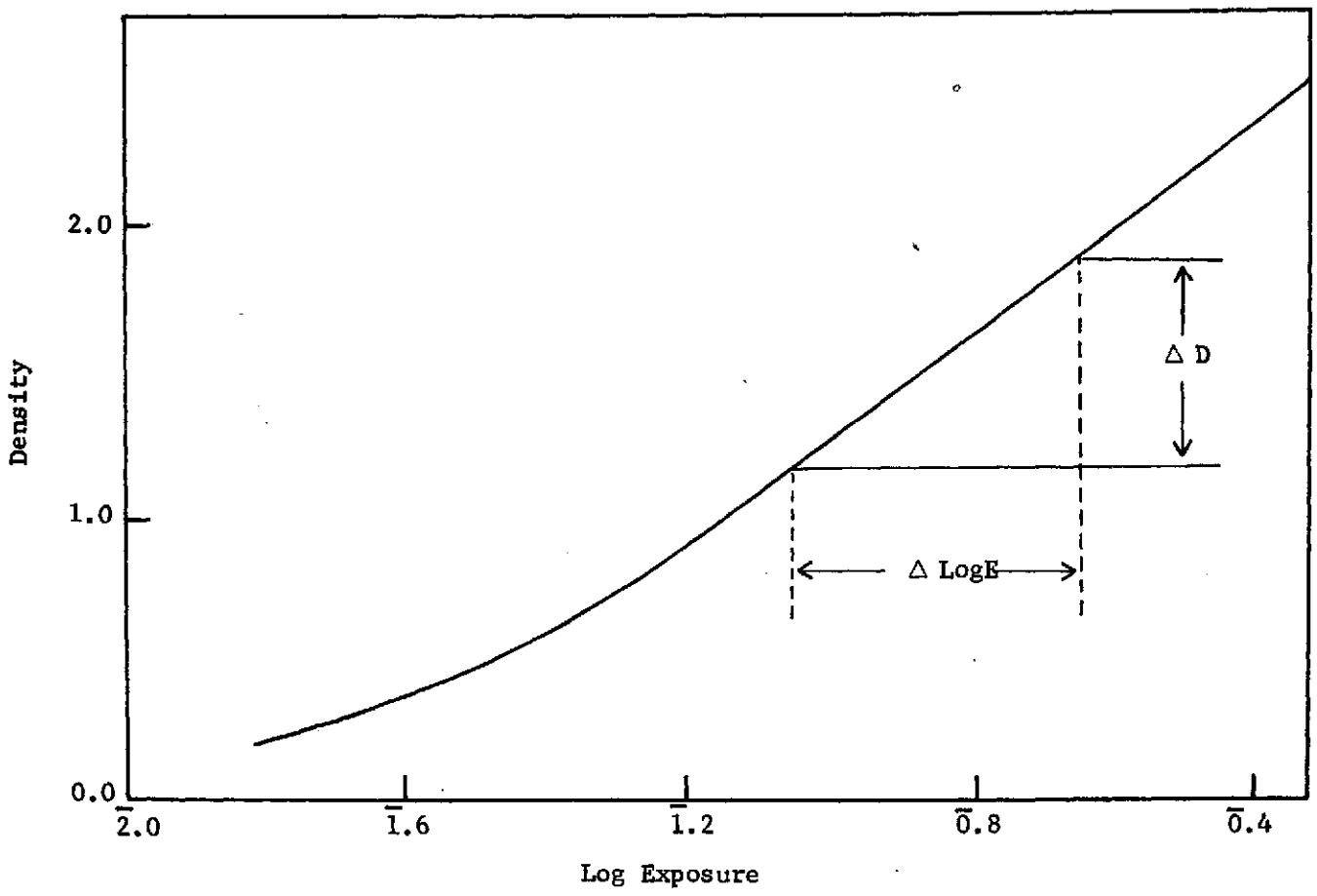

FIGURE III-4. The General Form of the γ-Curve for Negative Film.

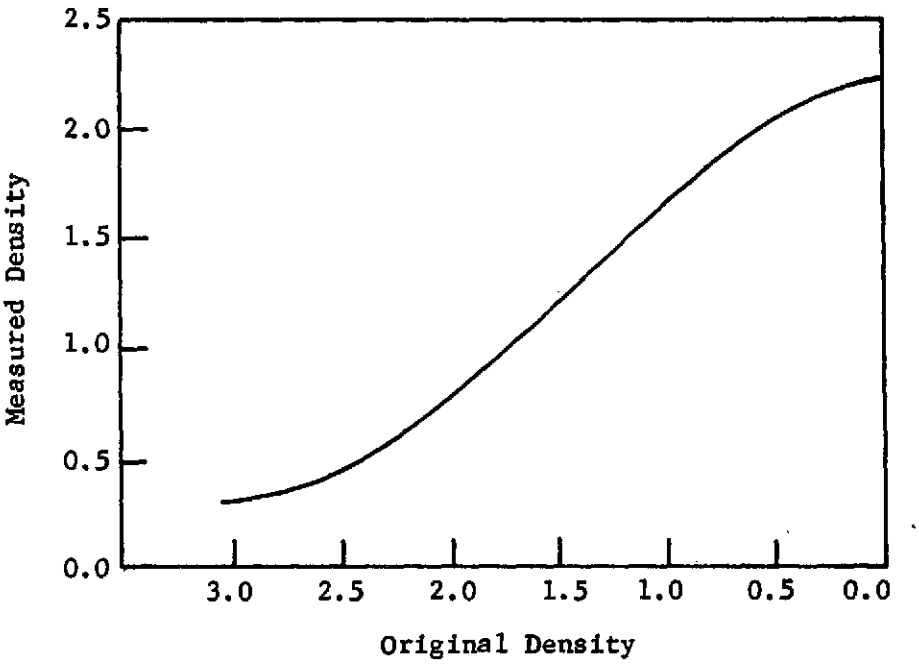

FIGURE III-5. The Determination of the γ-Curve for Negative Film.

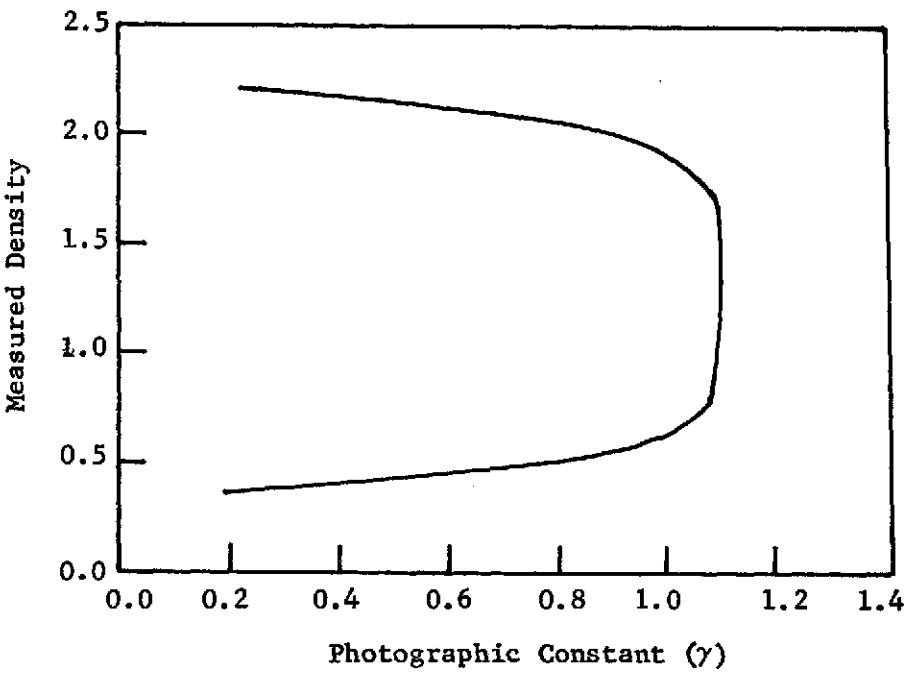

FIGURE III-6. The Derivative of the γ-Curve.

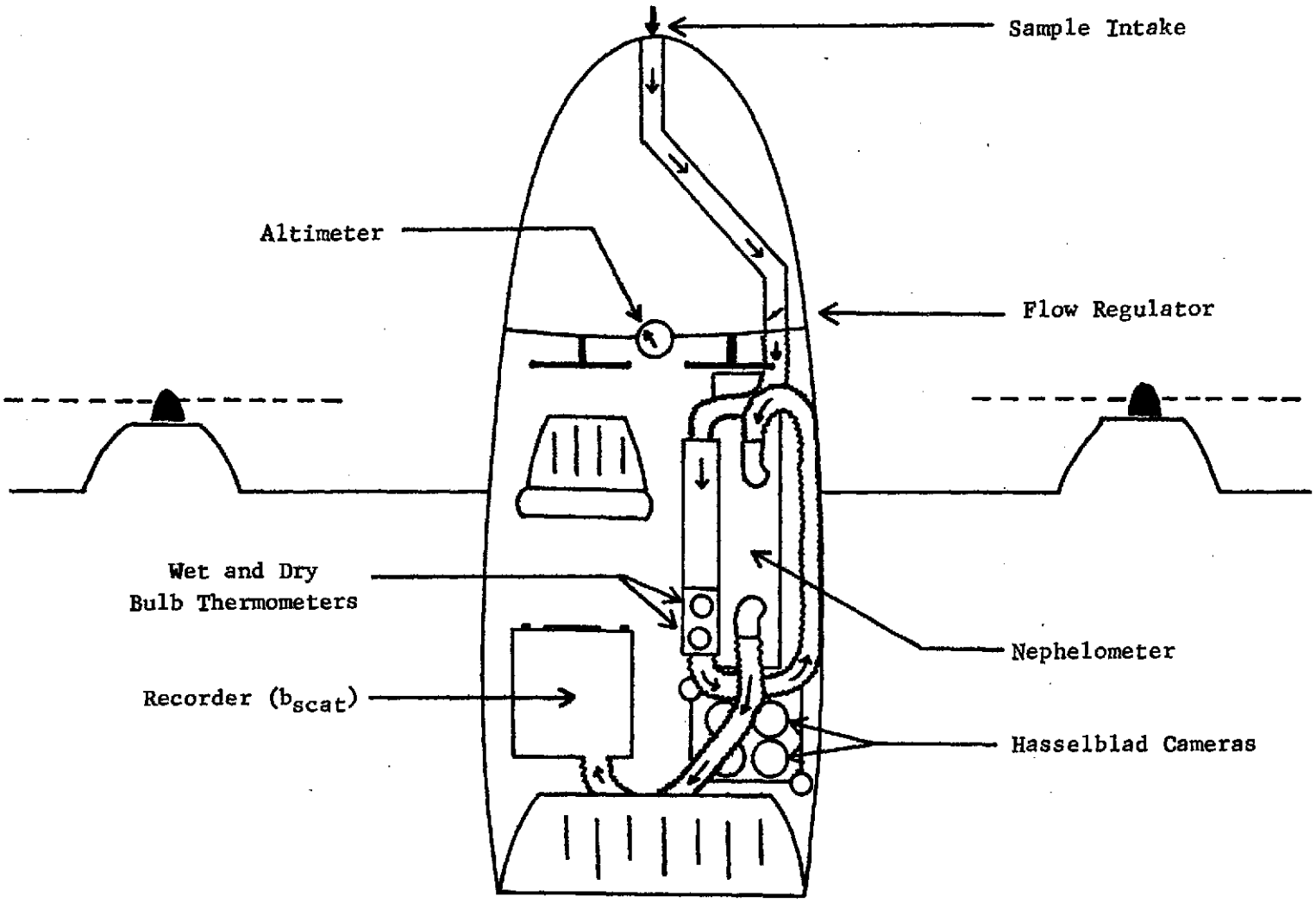

FIGURE IV-1. View of Airplane and the Experimental Apparatus.

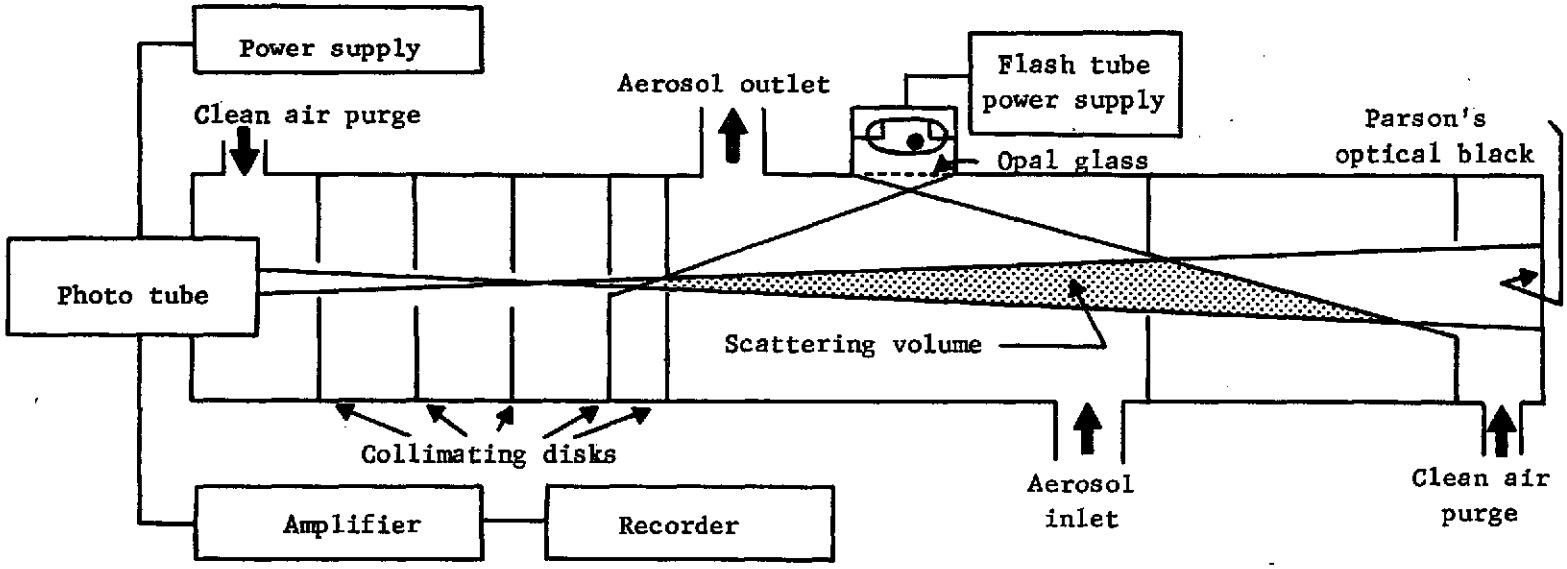

Figure IV-2. Schematic Diagram of the Integrating Nephelometer.

Source: Norman C. Ahlquist and Robert J. Charlson, "A New Instrument for Evaluating the Visual Quality of Air" (paper presented at the Pacific Northwest International Section of the Air Pollution Control Association, Seattle, Washington, 3-4 November, 1966).

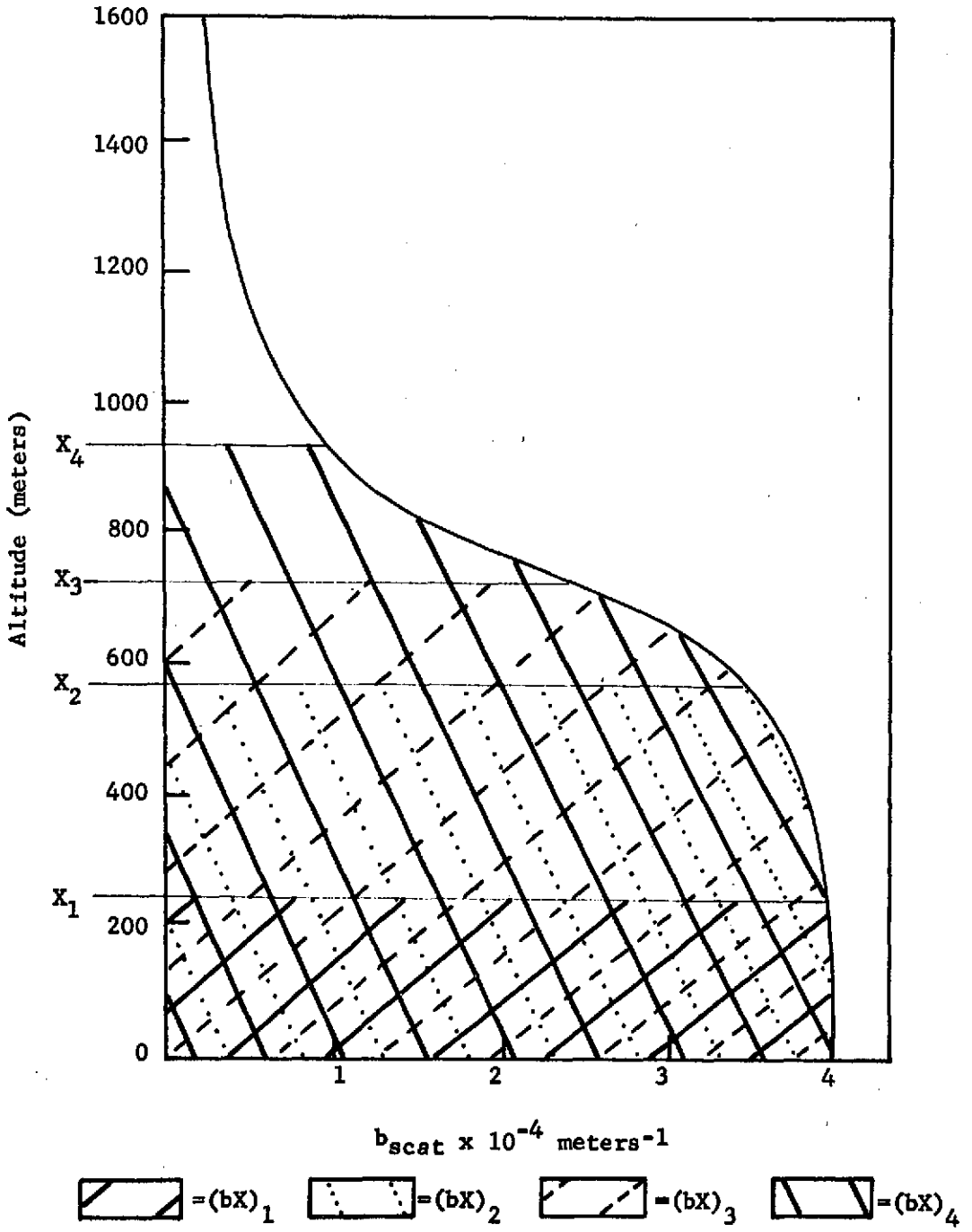

FIGURE IV-3. Calculation of the Accumulative bX by the Area Method.

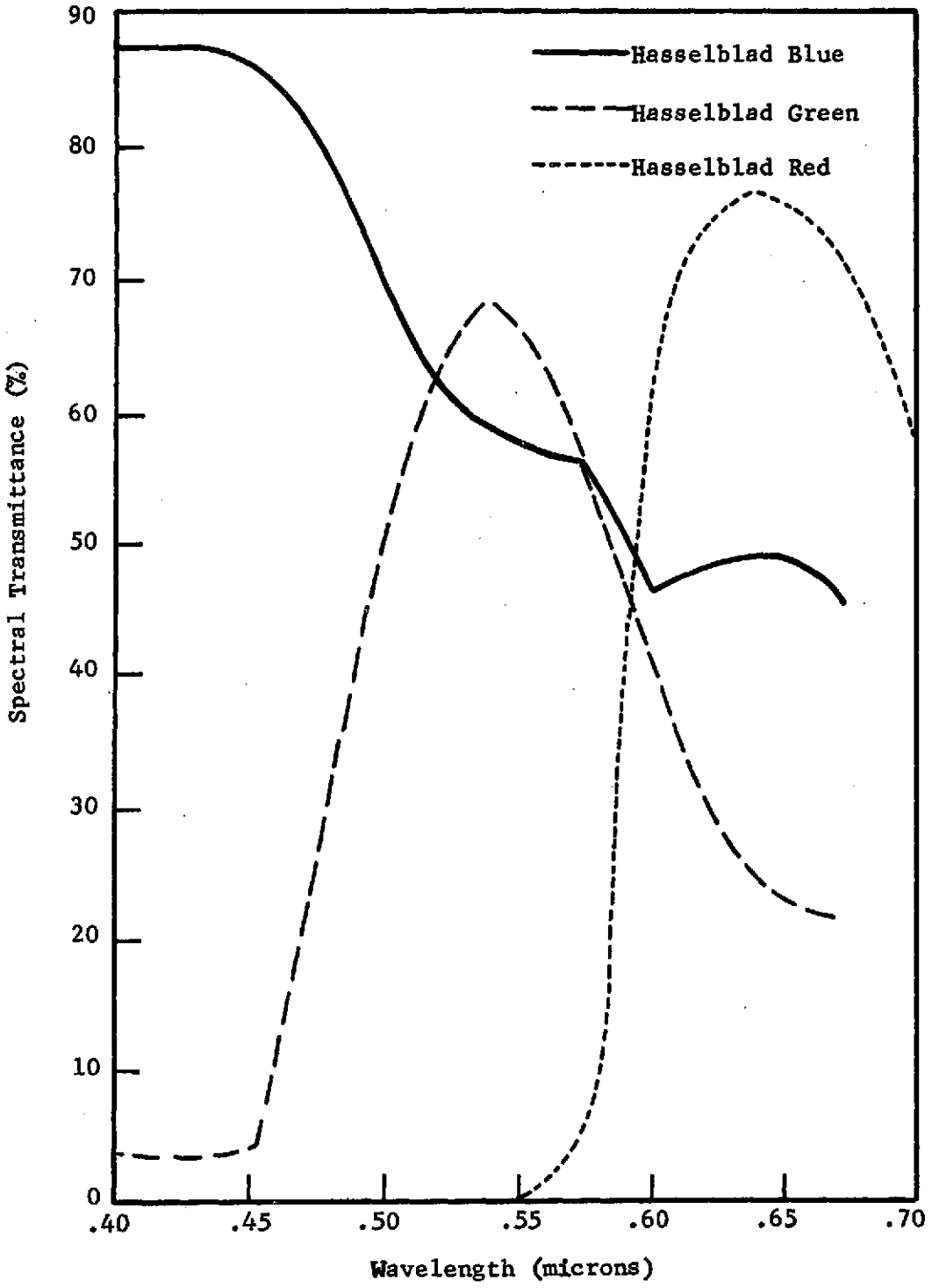

FIGURE IV-4. The Spectral Transmittance of the Camera Filters.

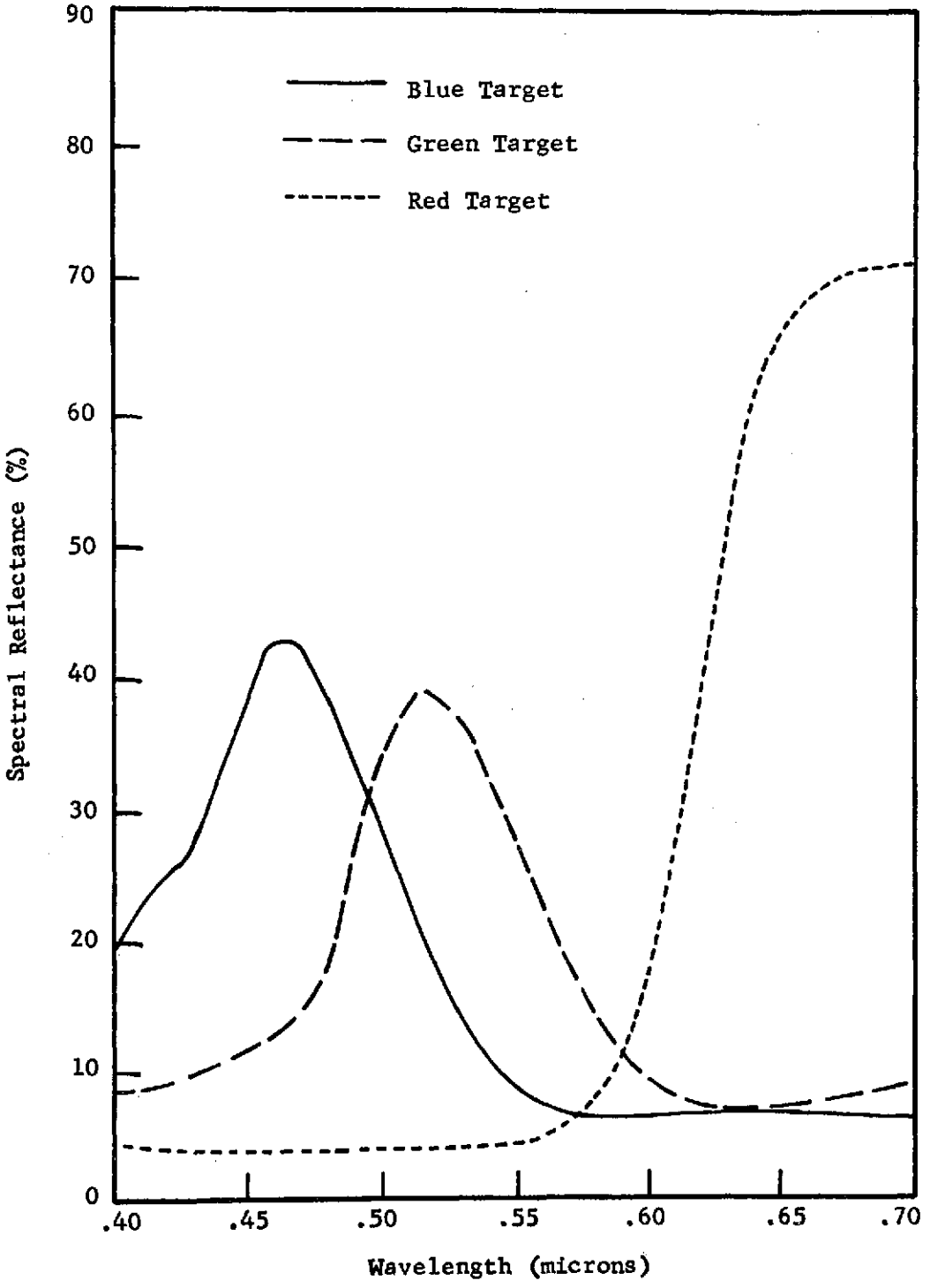

FIGURE IV-5. The Spectral Reflectance of the Three Colored Targets.

Figure IV-6A

Figure IV-6B

Figure IV-6. Photograph of (A) the Kodak Paper Gray Scale, and (B) the Kodak Photographic Step Tablet No.2.

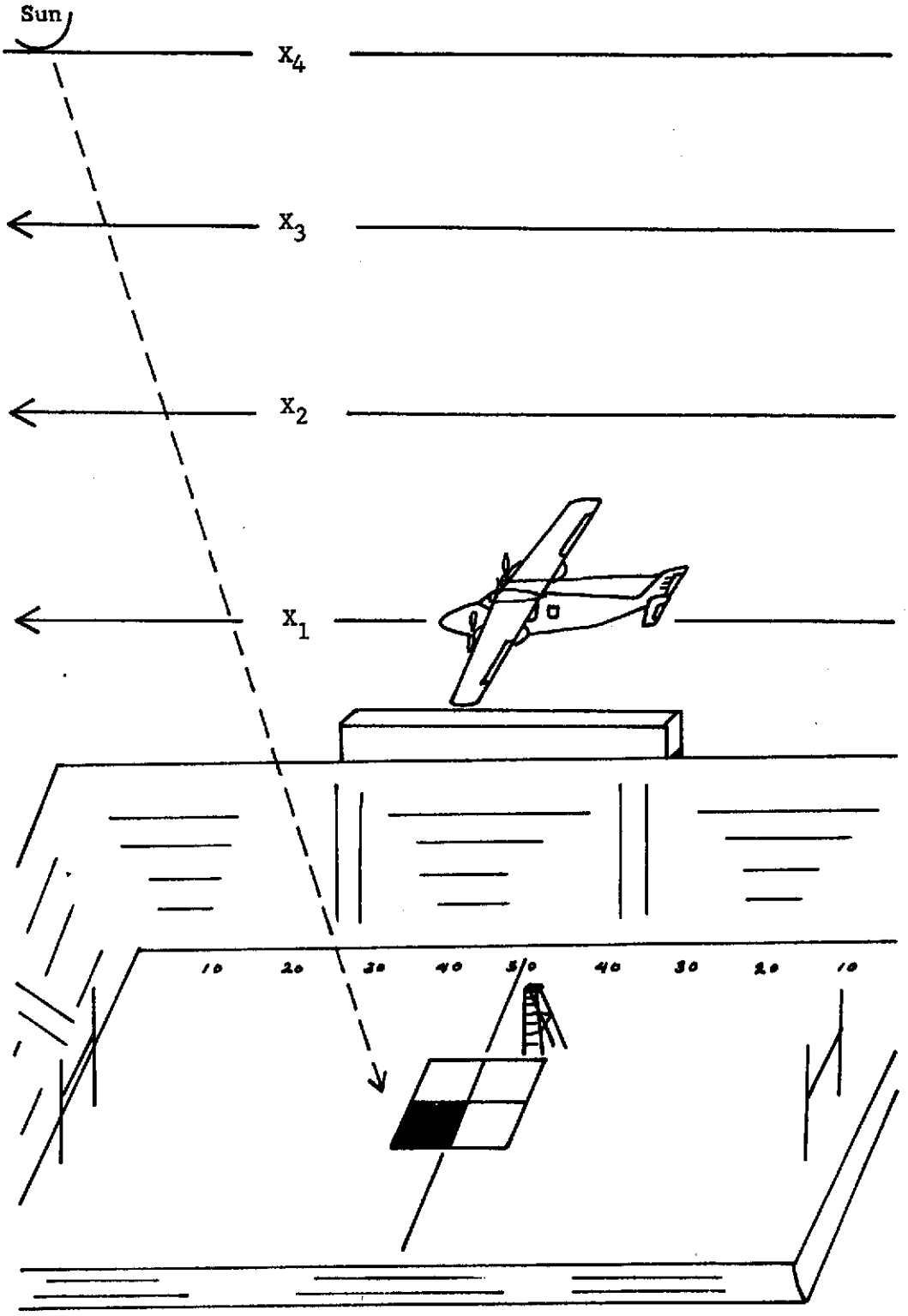

FIGURE IV-7. Diagram of Target Layout and Flight Pattern.

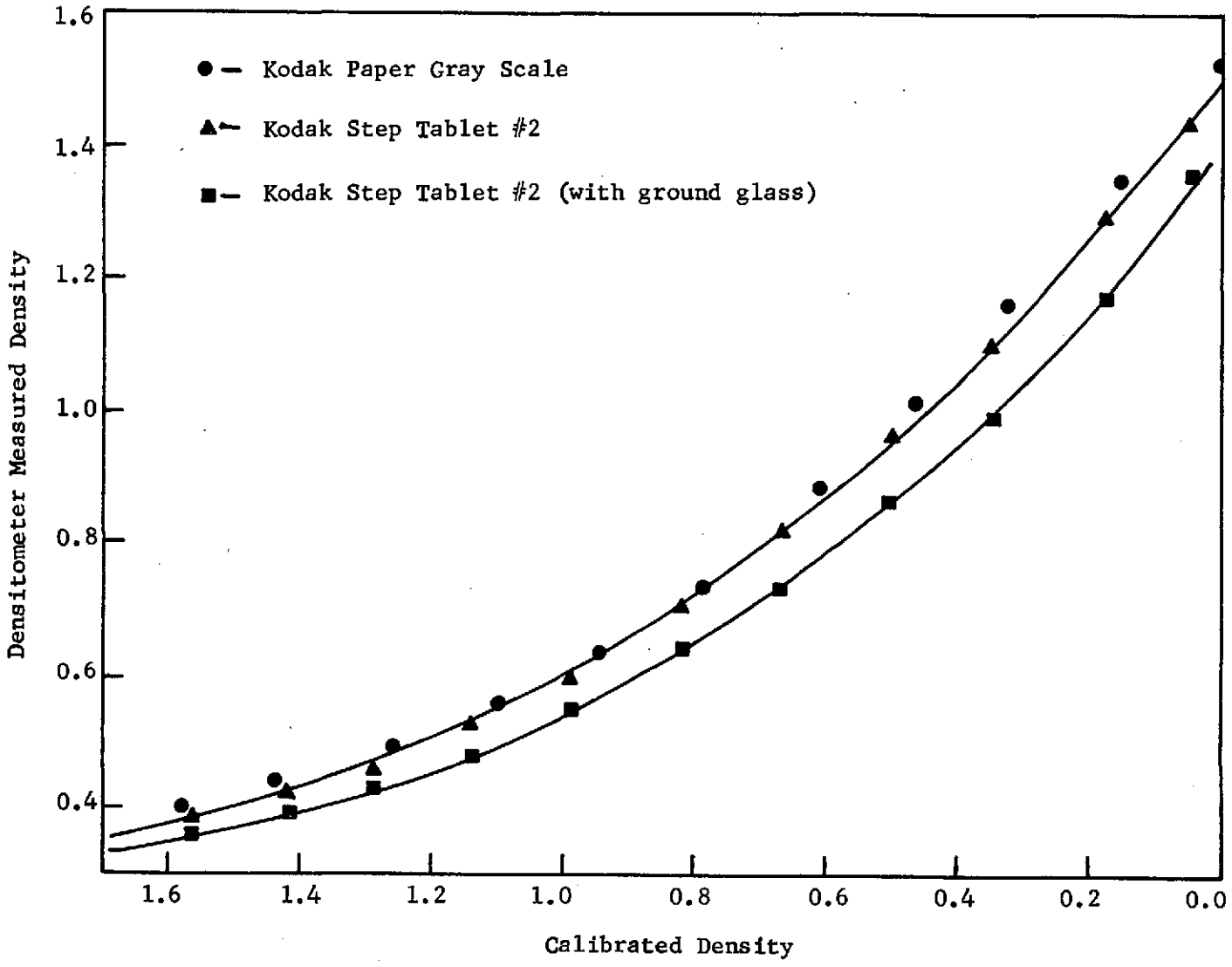

Figure IV-8. Comparison of Kodak Density Scales.

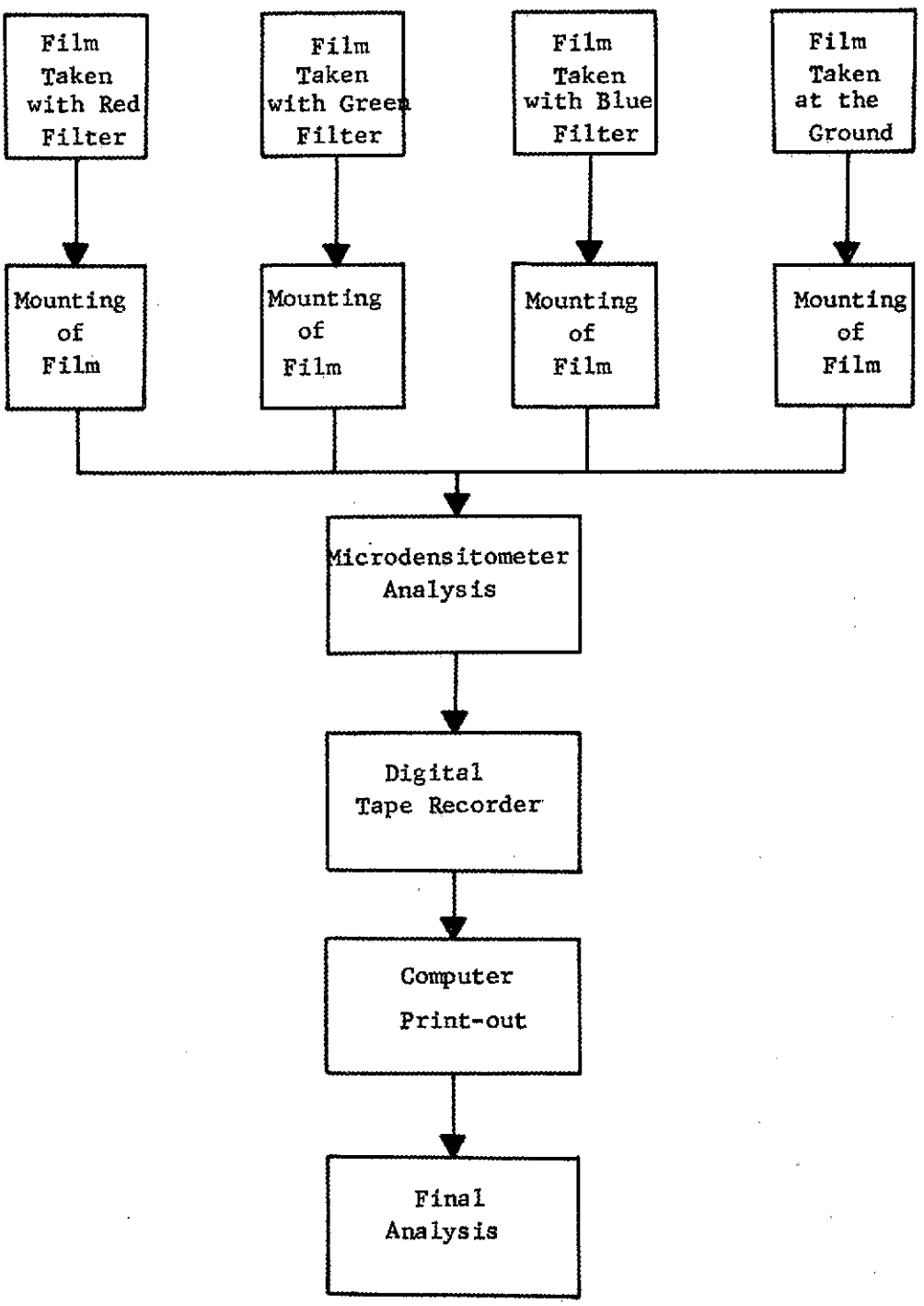

Figure IV-9. Flow Diagram for the Processes Involved in Film Analysis.

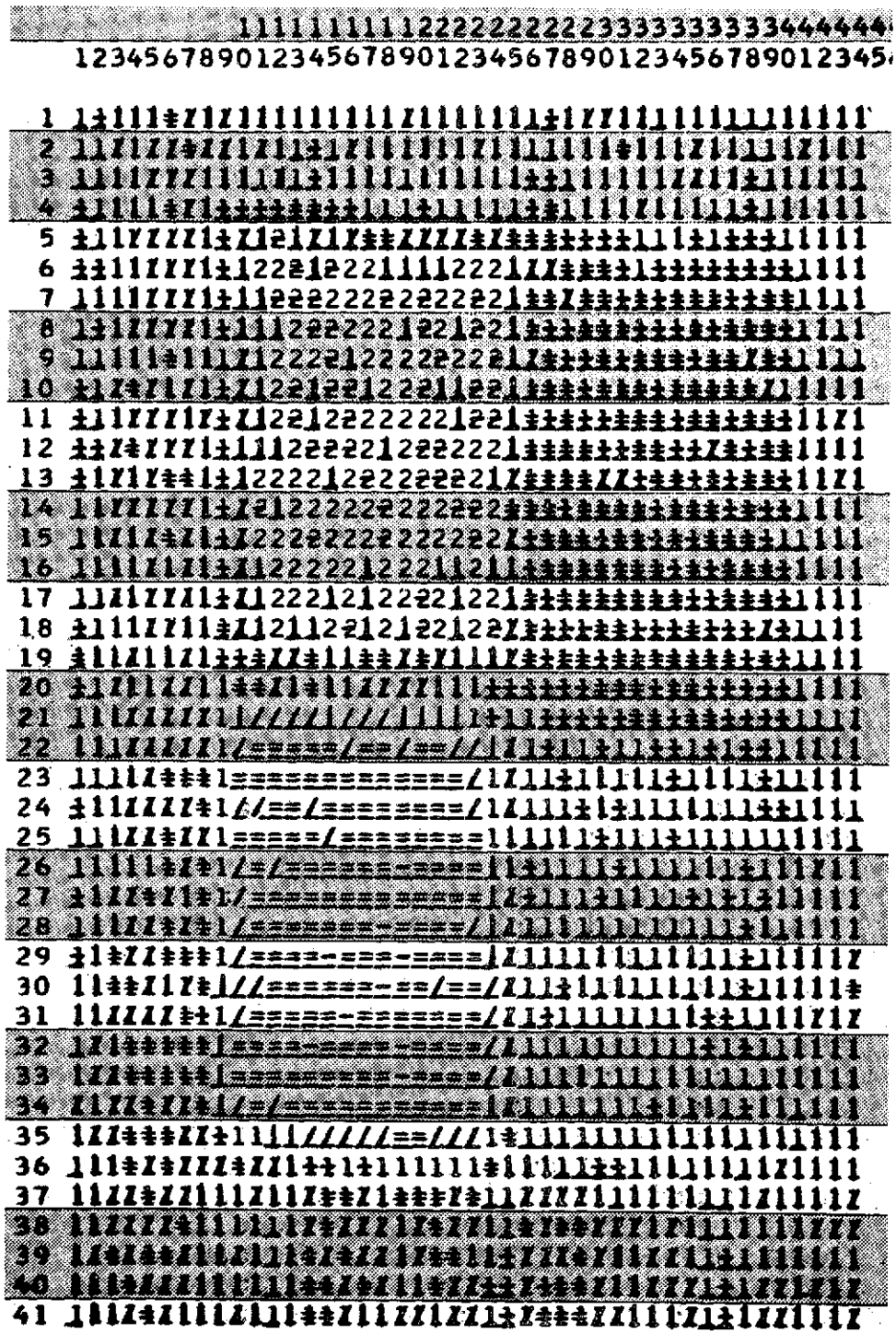

Figure IV-10. Photograph of the Computer Print-out Showing Some of the Symbols Used for Density.

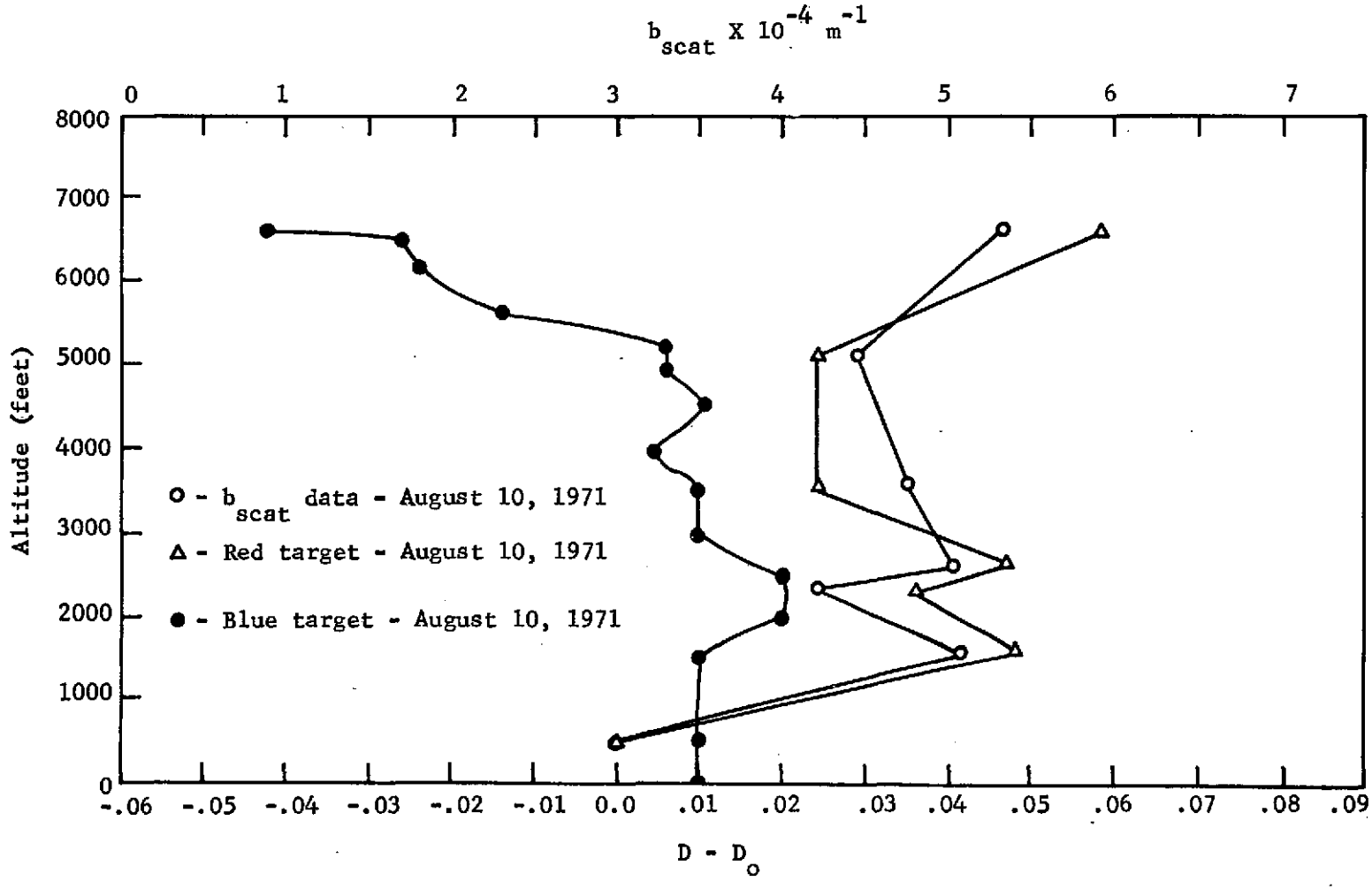

Figure V-1. Change in Density of Targets with Altitude for Flight of August 10, 1971.

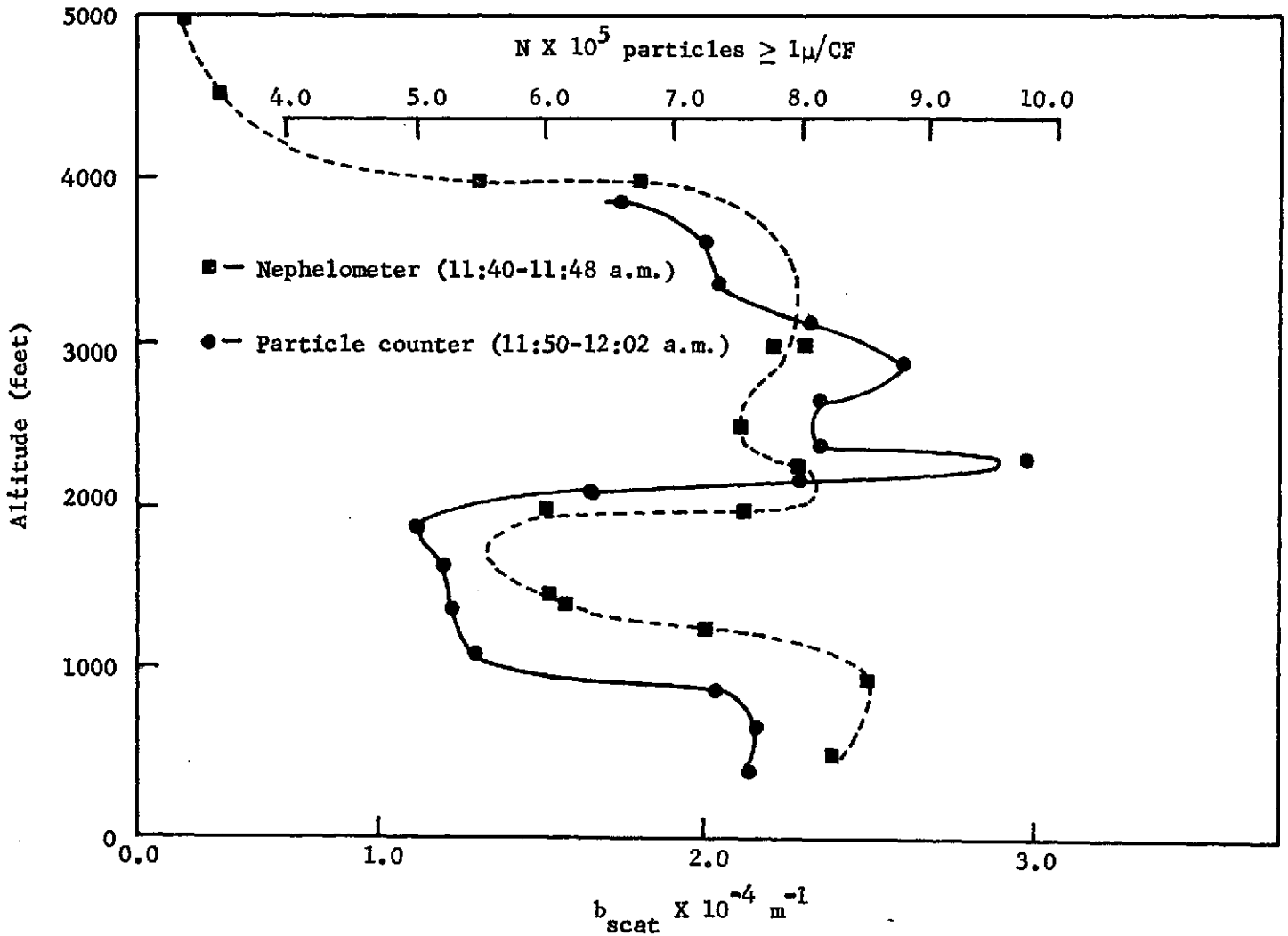

Figure V-2. Comparison of the Vertical Profiles of the Aerosol Particle Count and the Scattering Coefficient.

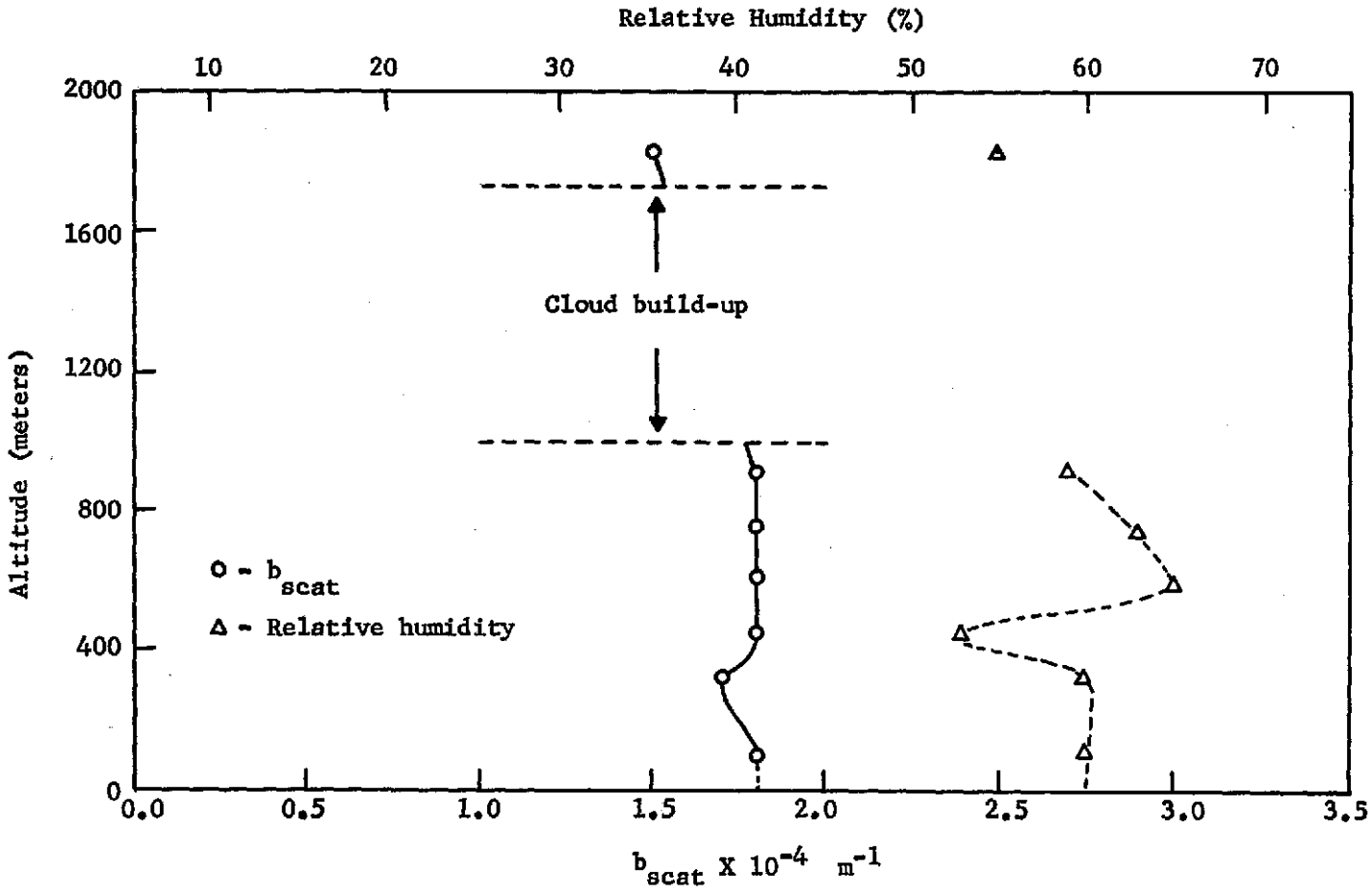

Figure V-3. Profiles of the Scattering Coefficient and the Relative Humidity for the June 30, 1972 Flight.

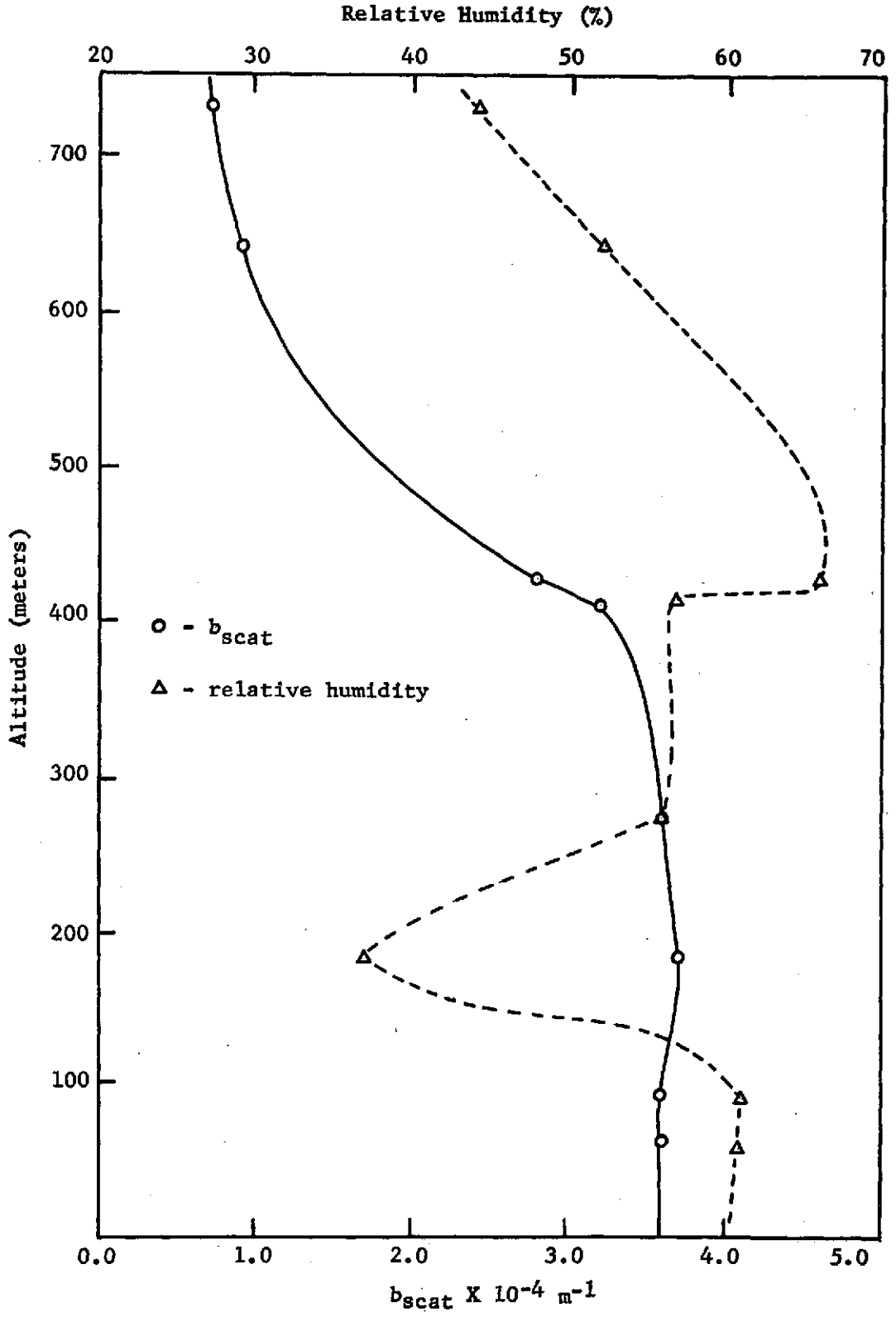

Figure V-4. Profiles of the Scattering Coefficient and the Relative Humidity for the July 12, 1972 Flight.

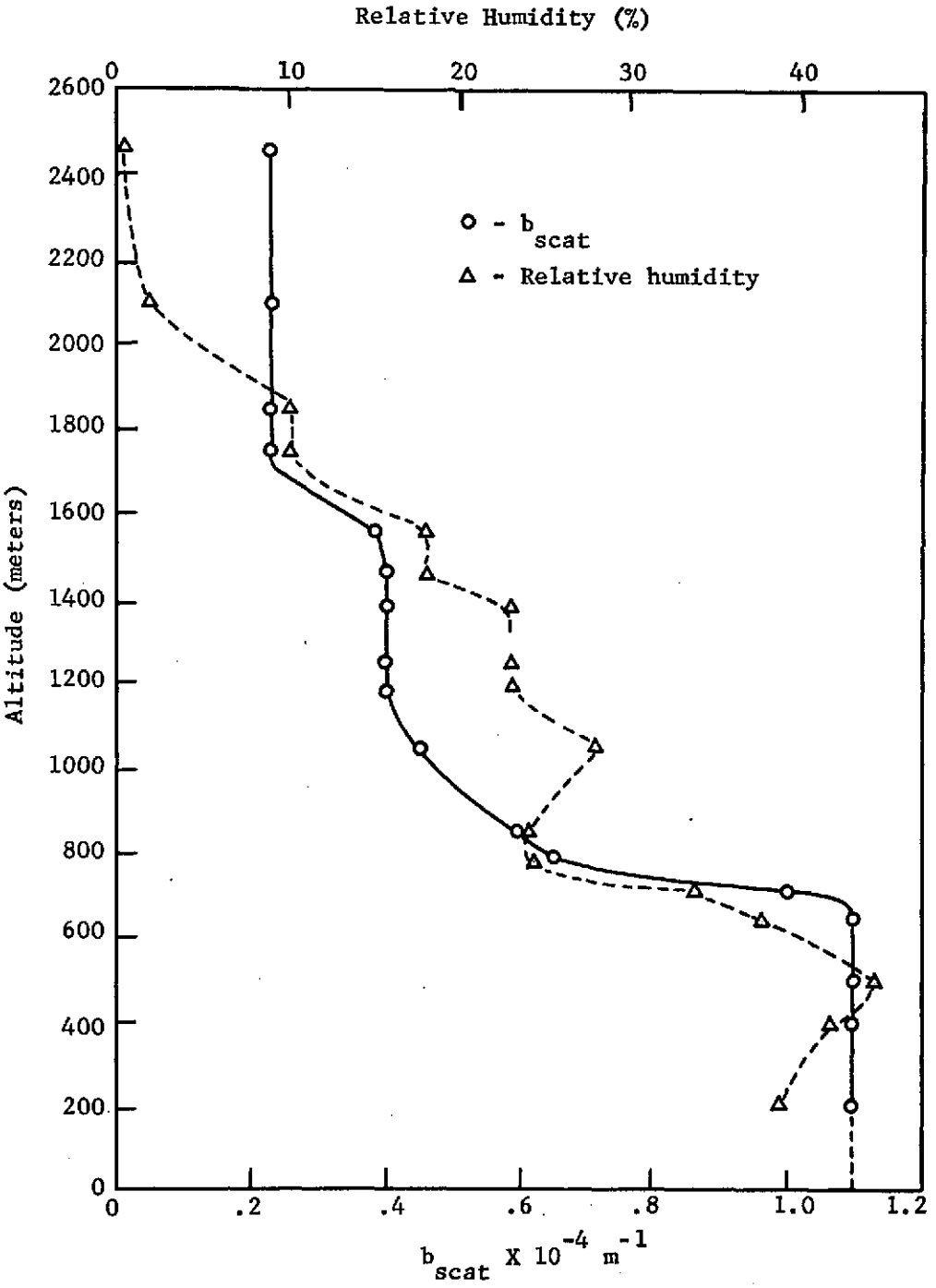

Figure V-5. Profiles of the Scattering Coefficient and the Relative Humidity for the November 6, 1972 Flight.

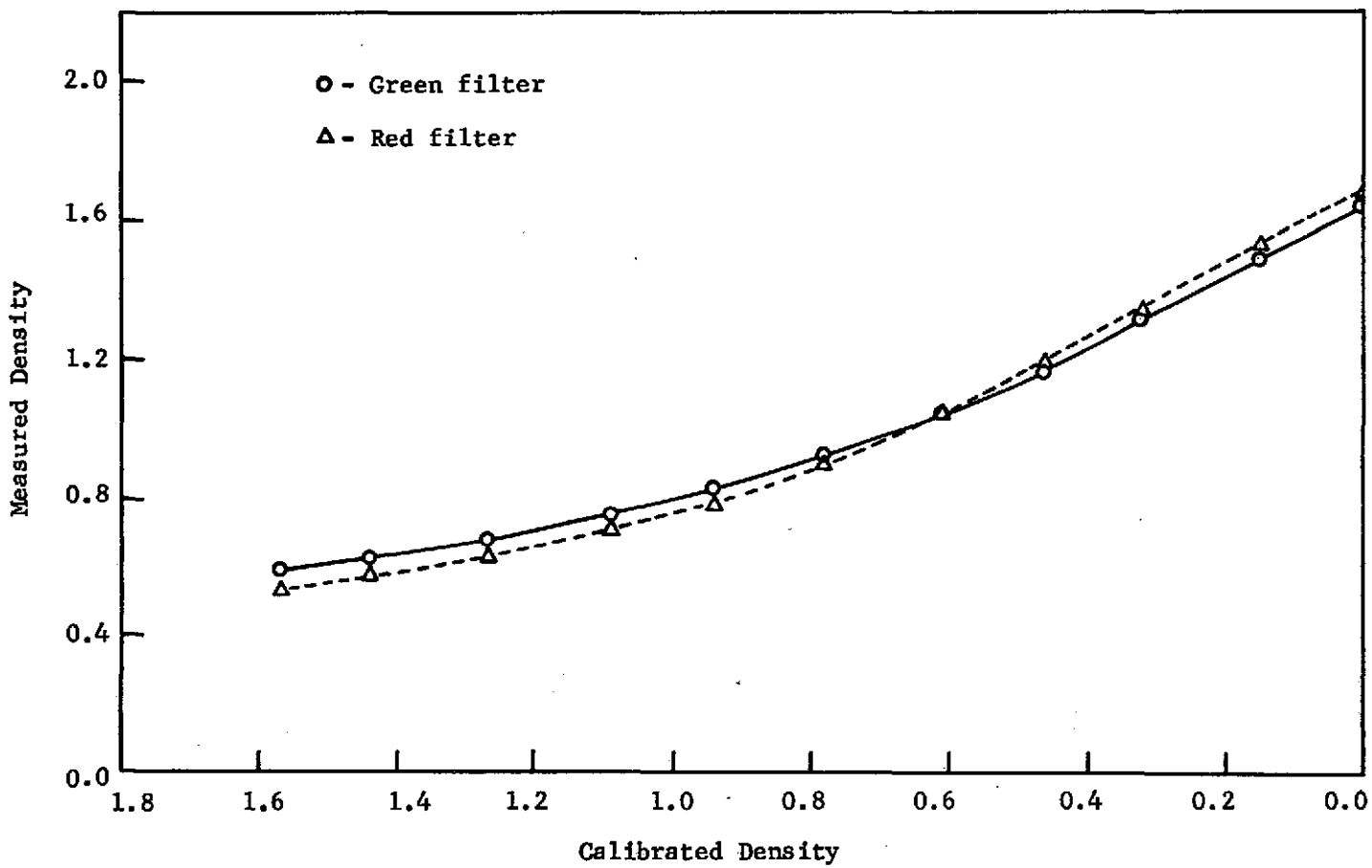

Figure V-6. The γ-Curves for the June 30, 1972 Flight.

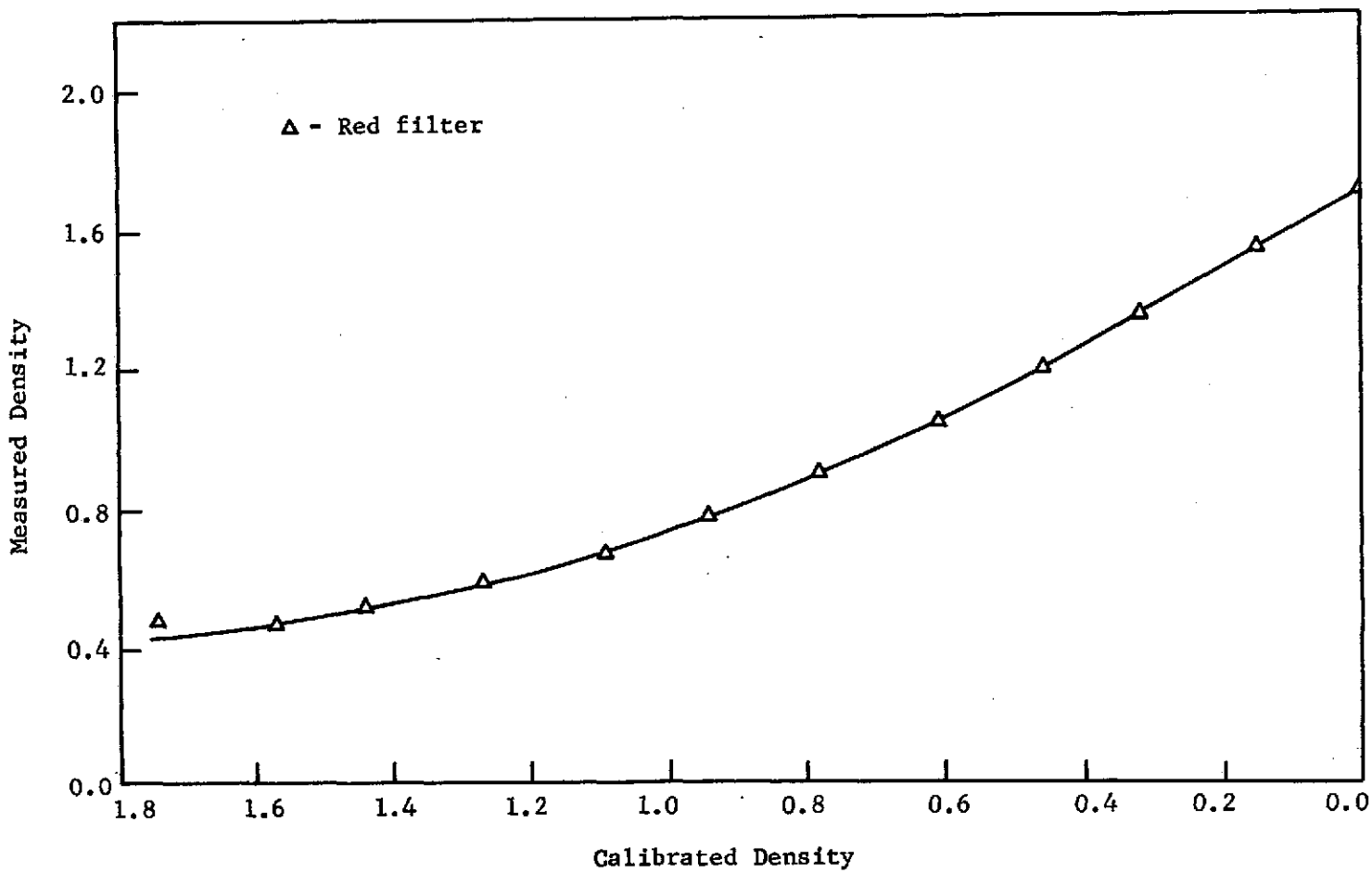

Figure V-7. The γ-Curve for the Red Filter on the July 12, 1972 Flight.

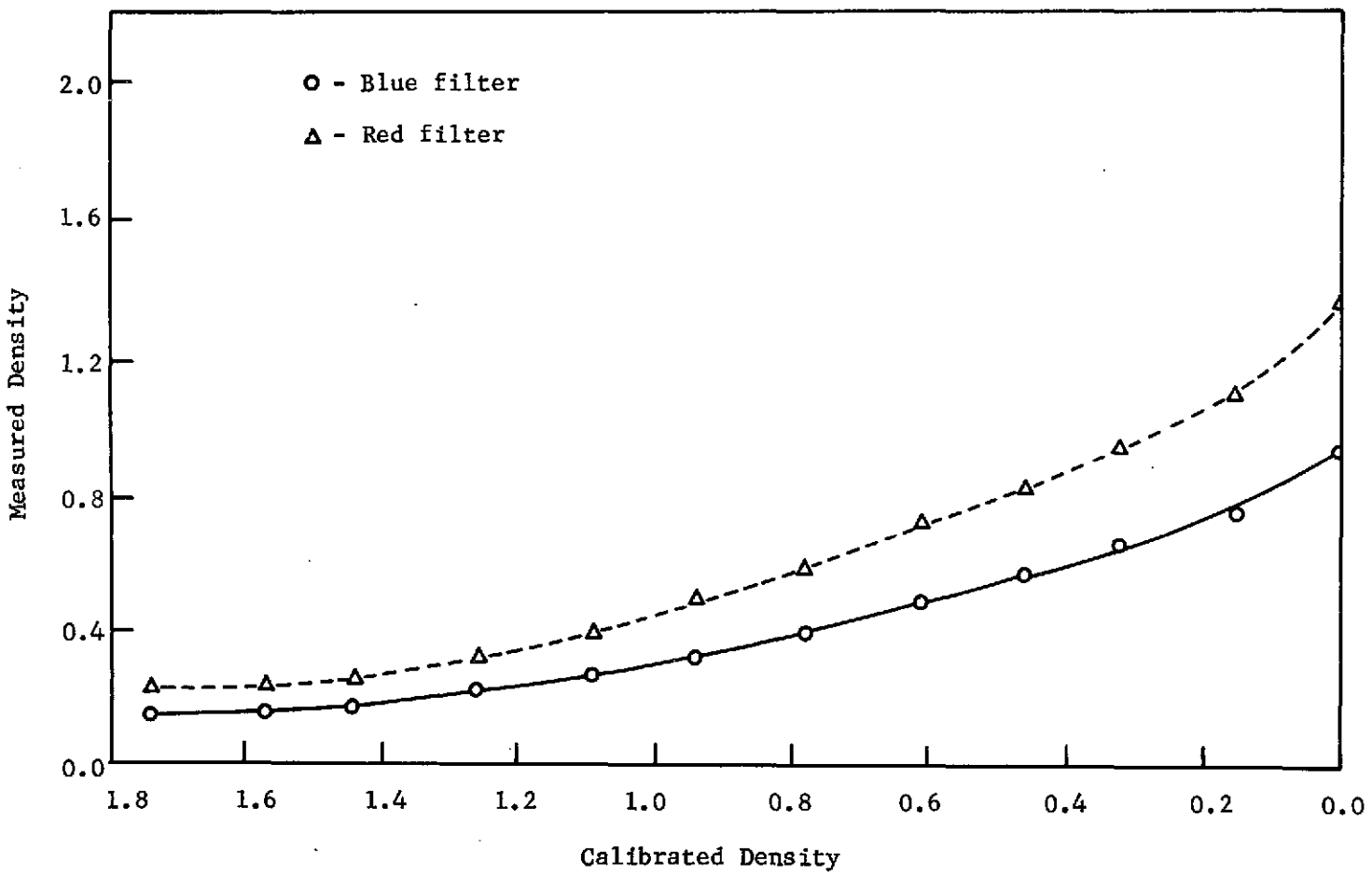

Figure V-8. The γ-Curves for the November 6, 1972 Flight.

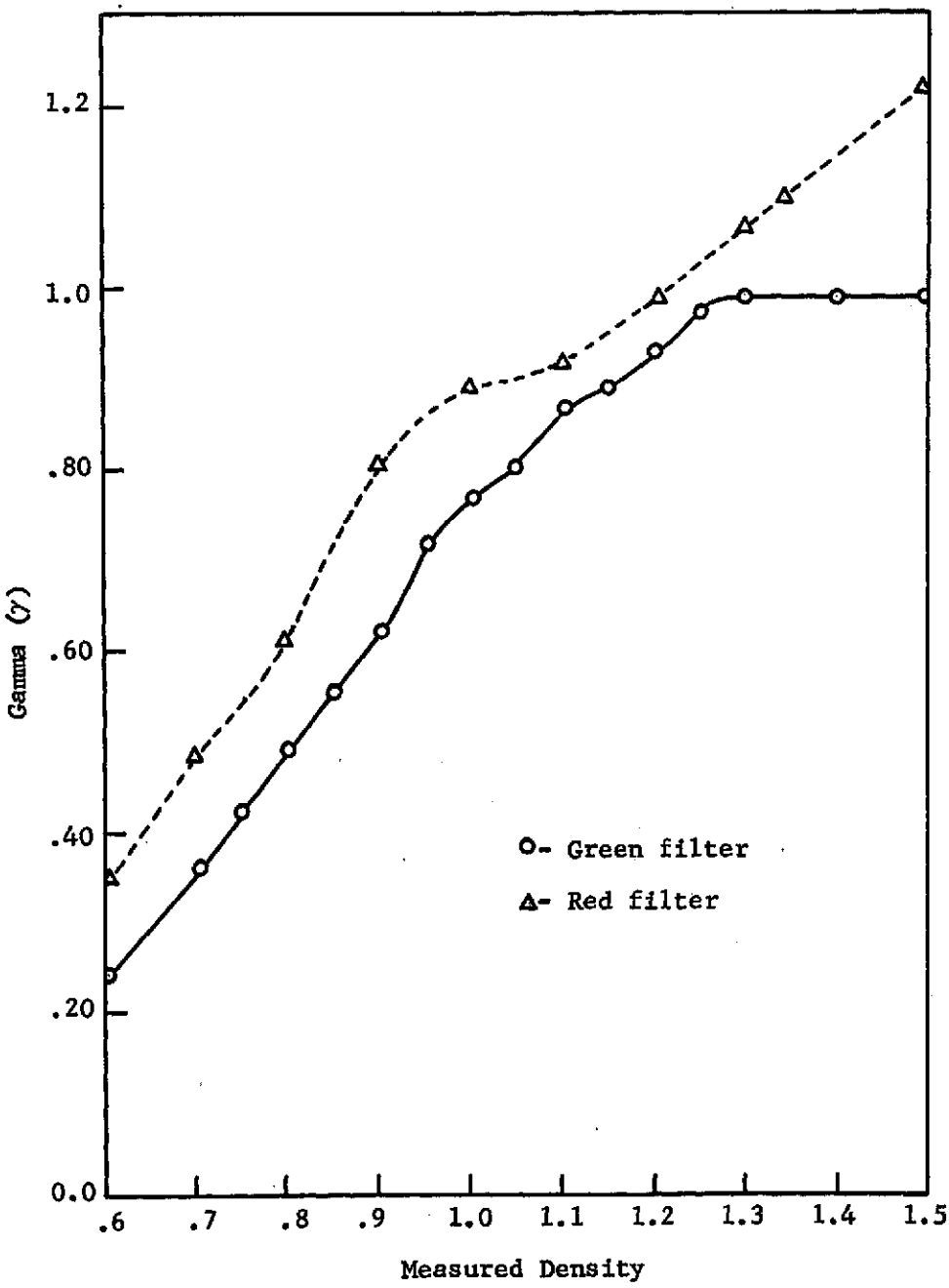

Figure V-9. Gamma for Each Measured Density for the June 30, 1972 Flight.

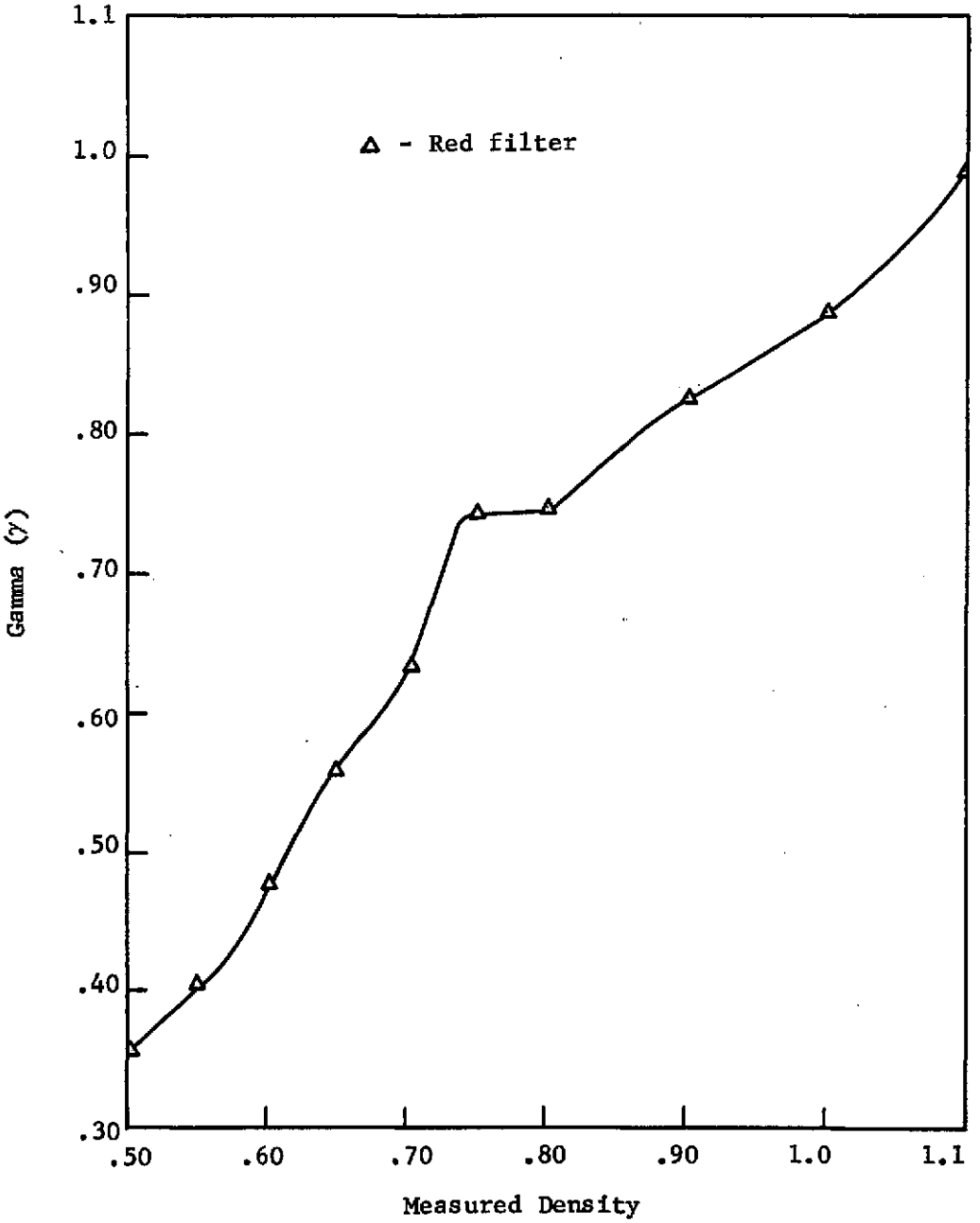

Figure V-10. Gamma for Each Measured Density for the July 12, 1972 Flight.

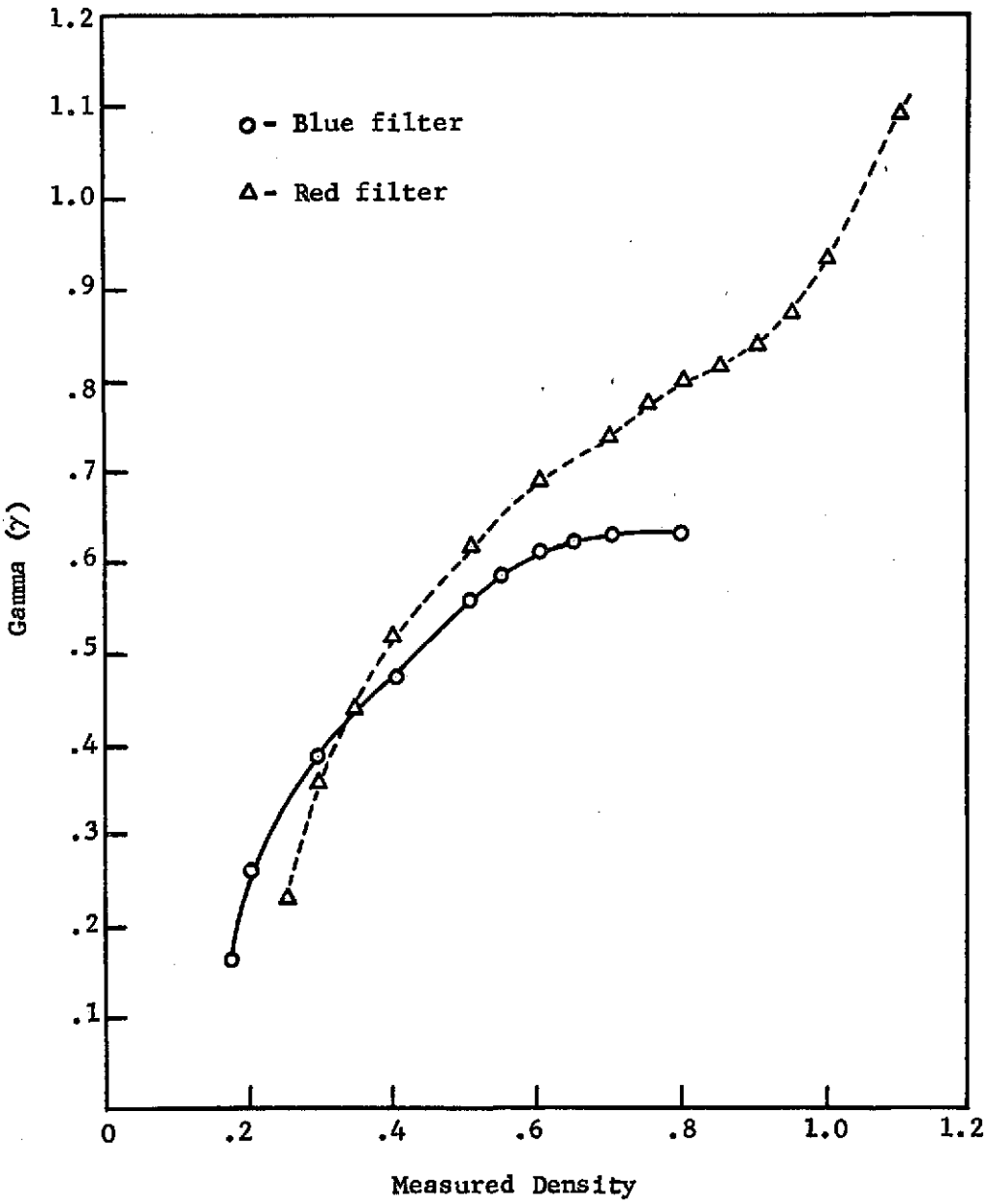

Figure V-11. Gamma for Each Measured Density for the November 6, 1972 Flight.

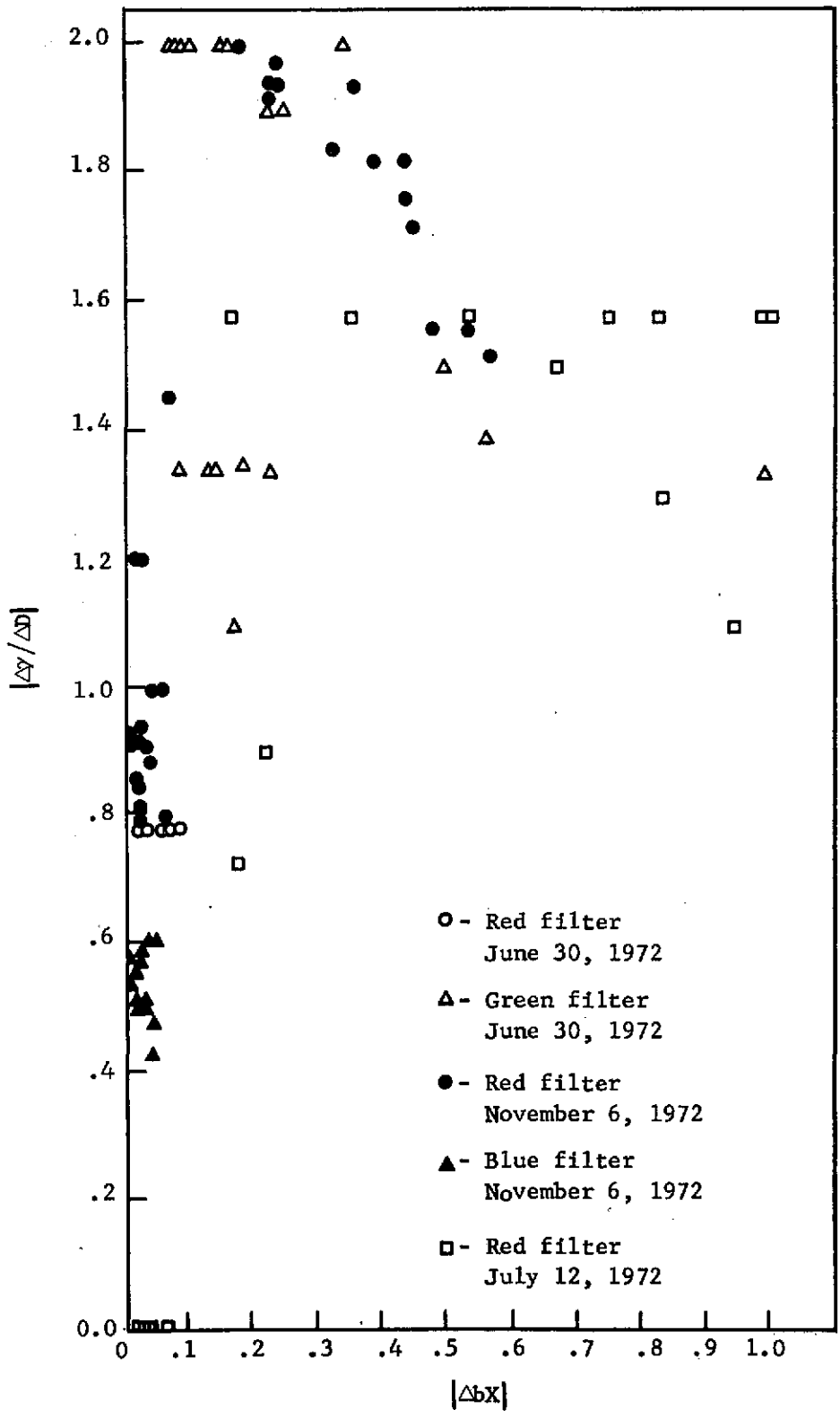

Figure V-12. Graph of $|\Delta y/\Delta D|$ versus $|\Delta bX|$ for All Flights.

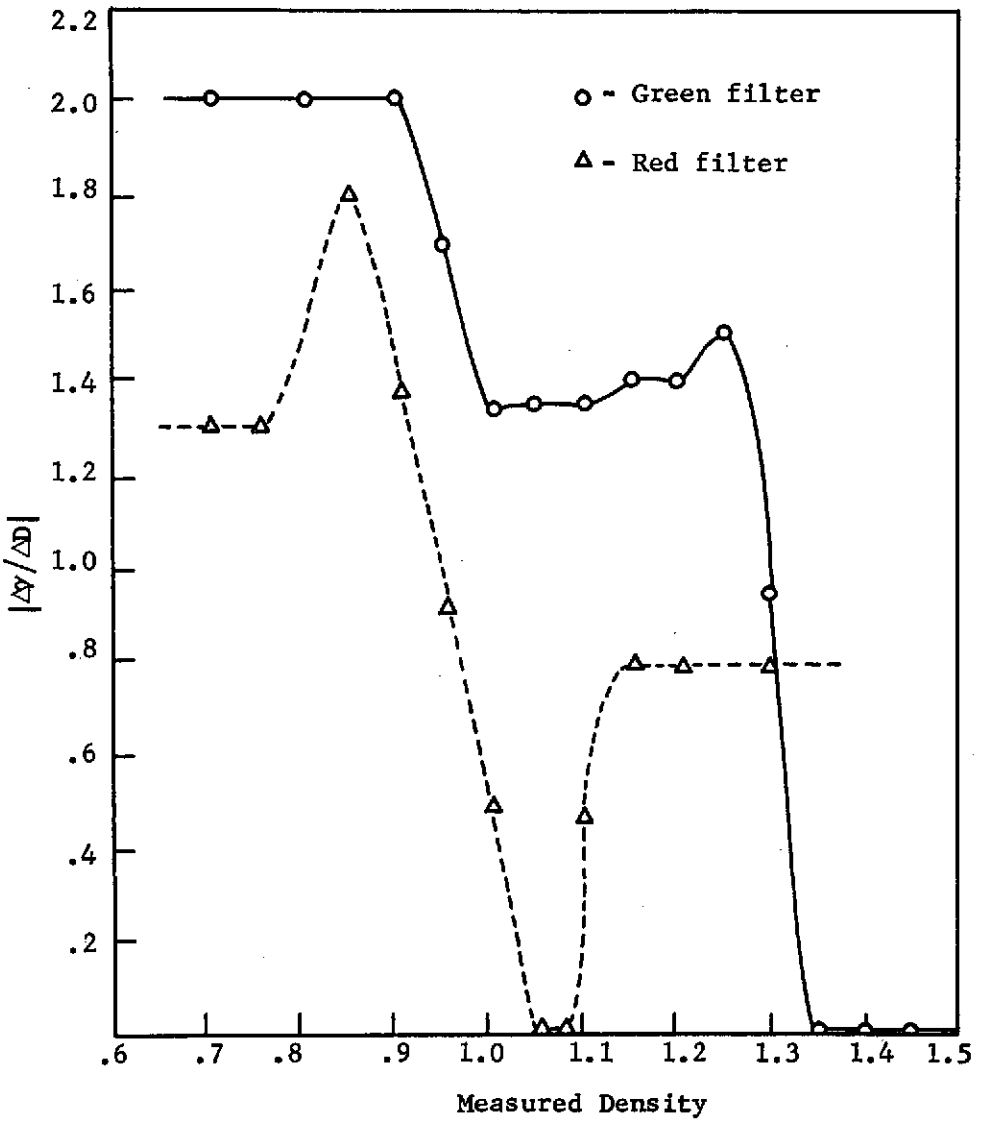

Figure V-13. Graph of $|\Delta\gamma/\Delta D|$ versus Measured Density for June 30, 1972 Flight.

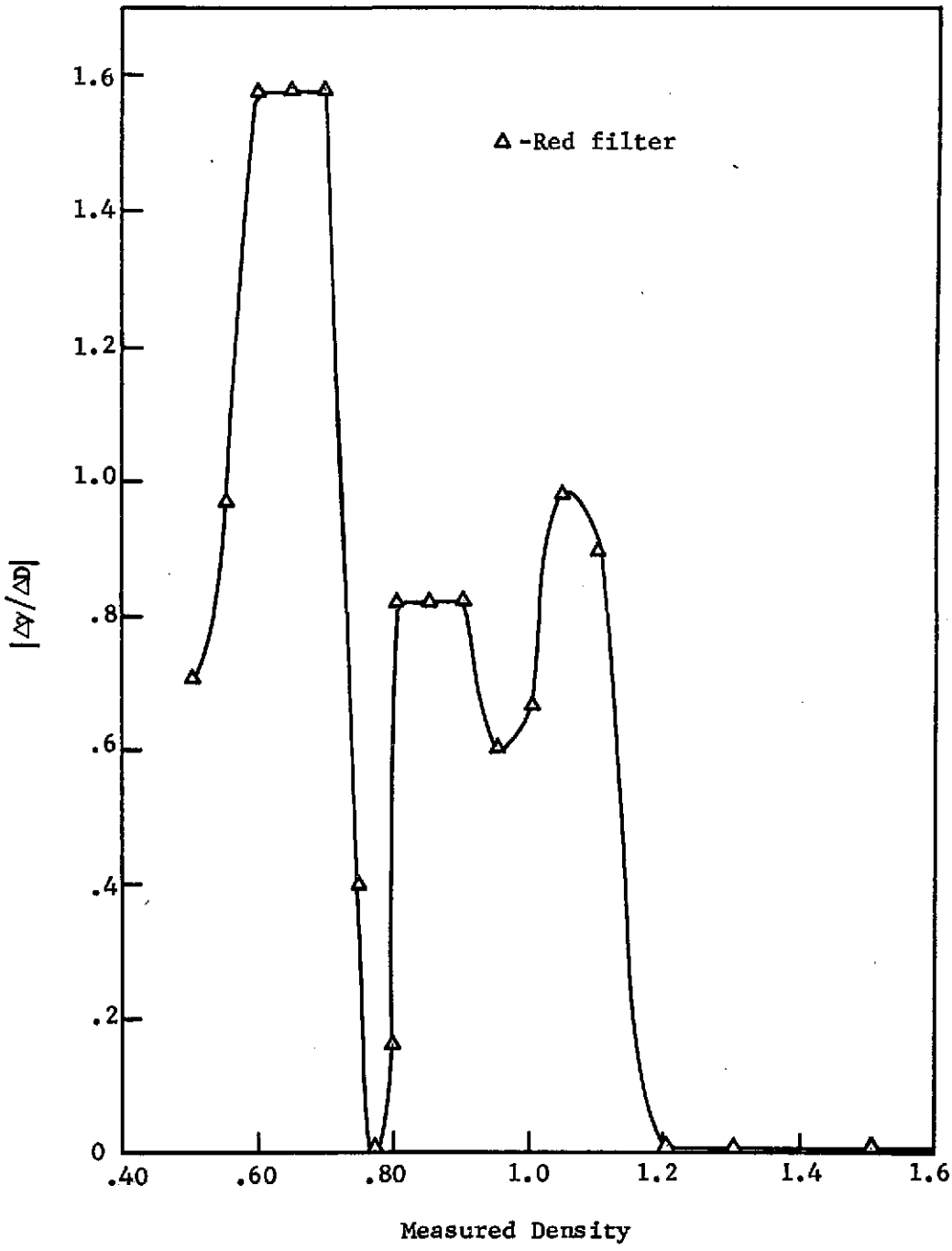

Figure V-14. Graph of $|\Delta\gamma/\Delta D|$ versus Measured Density for July 12, 1972 Flight.

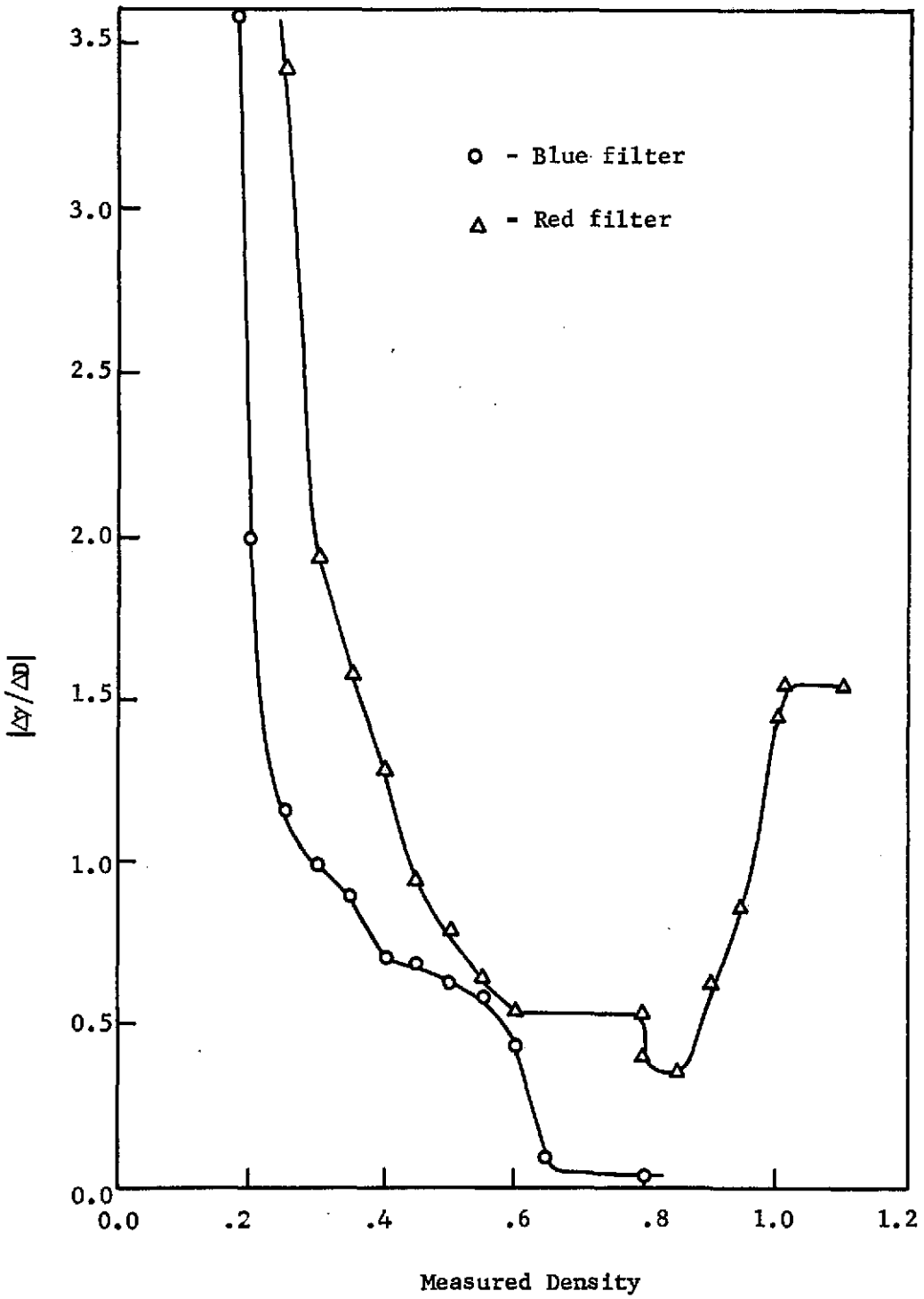

Figure V-15. Graph of $|\Delta y/\Delta D|$ versus Measured Density for November 6, 1972 Flight.

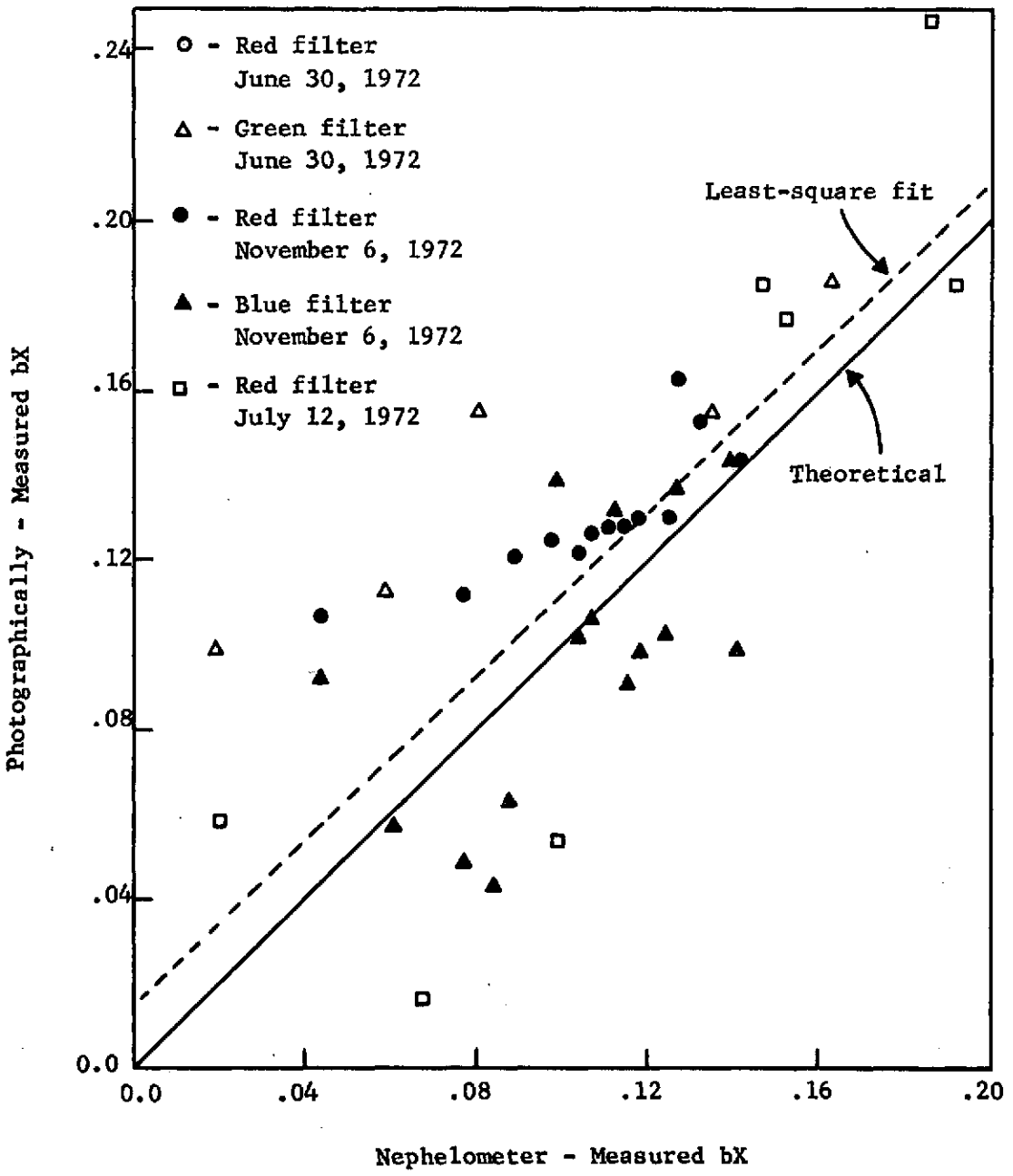

Figure V-16. Graph of bX Measured by Photography versus bX Measured by the Nephelometer for Data in Which $|\Delta\gamma/\Delta D| \leq 1.0$.